Supplemental information list

Supplemental Figures

Supplemental Experimental Procedures

Supplemental References

Supplemental Tables

A

Table GSEA of three alcohol and high fat fed mouse models

WD-fed *Ns5a* Tg mice vs WD-fed Non-Tg mice

NAME	ES	NES	NOM p-value
RB_DN.V1_UP	0.93	1.98	0.00
CAMP_UP.V1_UP	0.79	2.19	0.00
ACEVEDO_METHYLATED_IN_LIVER_CANCER_DN	0.83	1.68	0.03
ACEVEDO_TISSUE_ADJACENT_TO_LIVER_TUMOR_DN	0.55	1.51	0.05
CAVARD_LIVER_CANCER_MALIGNANT_VS_BENIGN	0.81	1.49	0.05
LEE_LIVER_CANCER_ACOX1_UP	0.93	1.48	0.05
BENPORATH_NANOG_TARGETS	0.68	1.49	0.05

Alcohol-fed *Ns5a* Tg mice vs. Alcohol-fed Non-Tg mice

NAME	ES	NES	NOM p-value
SHETH_LIVER_CANCER_VS_TXNIP	0.80	1.87	0.00
HSIAO_LIVER_SPECIFIC_GENES	0.53	1.62	0.02
BENPORATH_NANOG_TARGETS	0.68	1.26	0.02
BEIER_GLIOMA_STEM_CELL_UP	0.7	1.29	0.05
LEE_LIVER_CANCER_SURVIVAL_UP	0.60	1.48	0.05
ACEVEDO_LIVER_TUMOR_VS_ NORMAL_ADJACENT_TISSUE_UP	0.56	0.90	0.05

Alcohol-fed HCV *Core* Tg vs Alcohol-fed Non-Tg mice

NAME	ES	NES	NOM p-value
ACEVEDO_TISSUE_ADJACENT_ TO_LIVER_TUMOR_DN	0.59	1.47	0.00
ATF2_UP.V1_DN	0.91	1.49	0.01
WOO_LIVER_CANCER_RECURRENCE_DN	0.73	1.62	0.02
CYCLIN_D1_KE_.V1_UP	0.87	1.44	0.04
BENPORATH_NANOG_TARGETS	0.69	1.20	0.04
WOO_LIVER_CANCER_RECURRENCE_DN	0.63	1.52	0.05
CYCLIN_D1_UP.V1_UP	0.87	1.43	0.05
HOSHIDA_LIVER_CANCER_SUBCLASS_S3	0.61	1.46	0.05

B

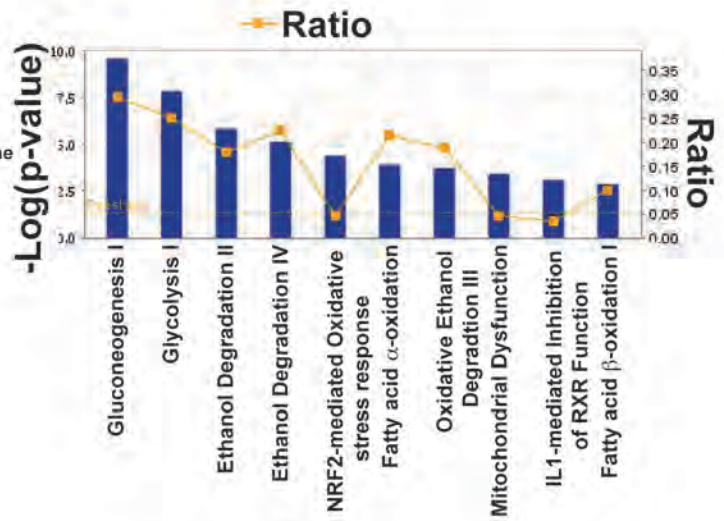

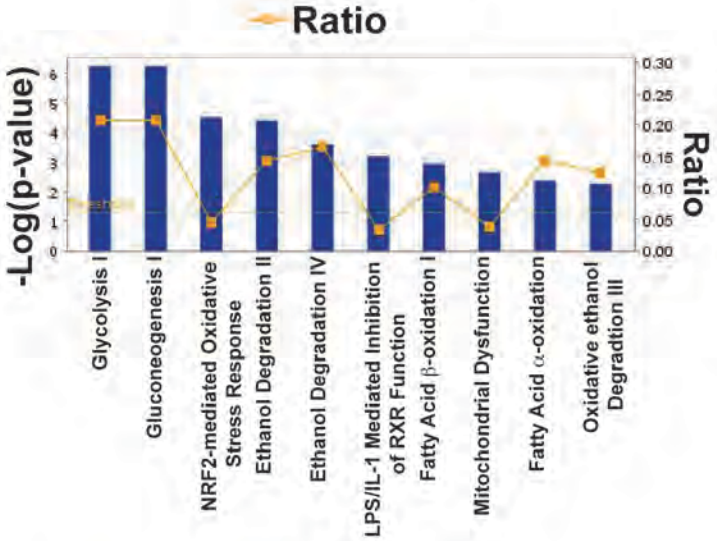

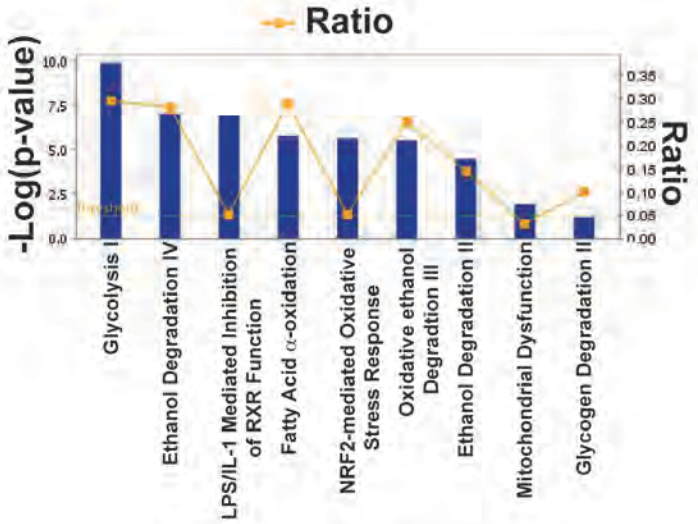

Figure S1 Continued
Chen *et al.*

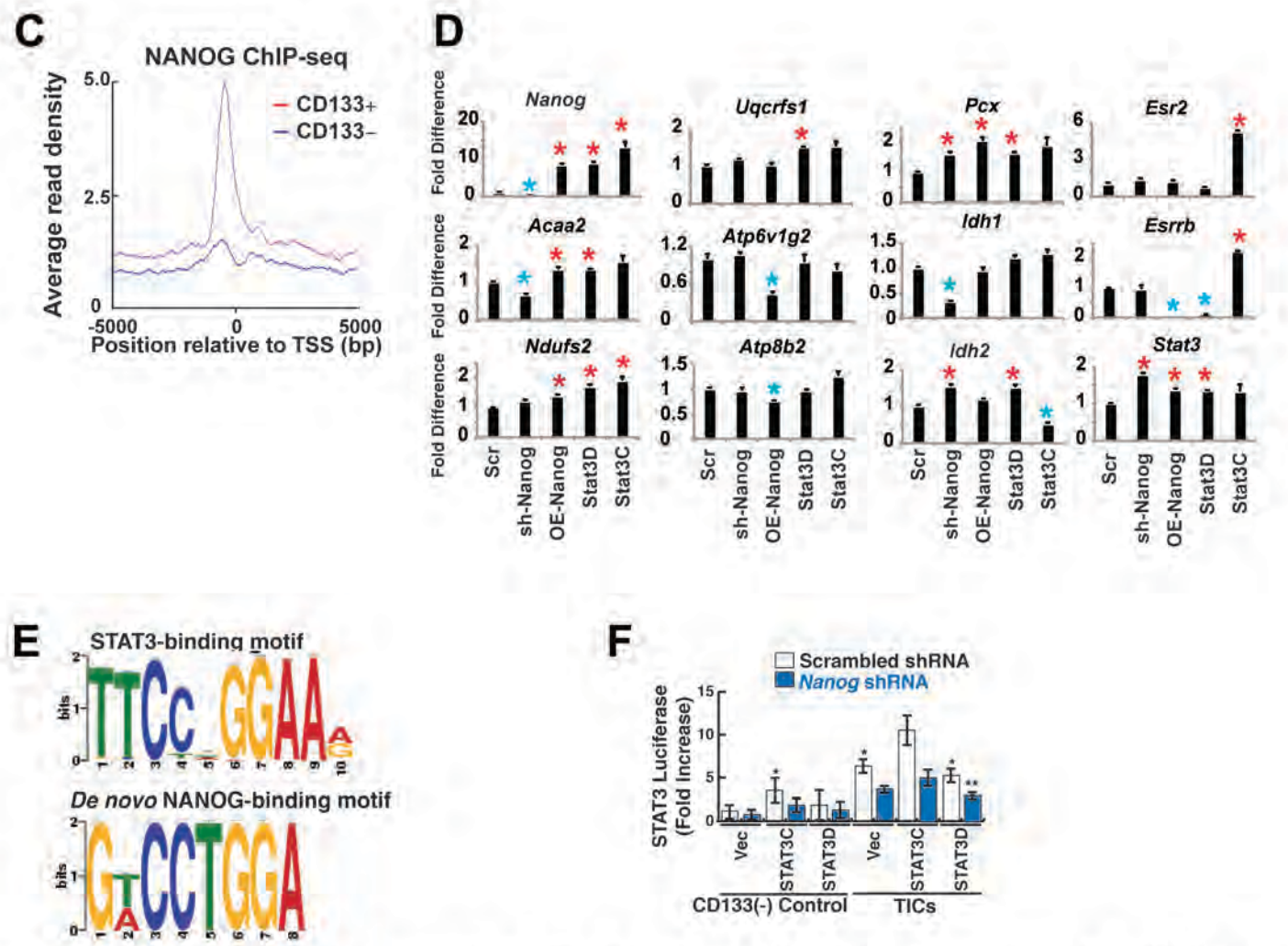

Fig. S1 (Related to Fig. 1). Pathway analysis of proteomics of different liver disease models and validation studies of NANOG target genes identified by NANOG ChIP-seq.

(**A**) Canonical pathways by proteomic analysis affected in tumor tissues of three different liver disease models. Note: NANOG-target genes are tightly linked to all three different HCC mouse models.

(**B**) Canonical pathways affected in diseased livers in three different liver disease models.

(**C**) NANOG enrichment proximal to initiation site of gene promoters in CD133(+) TICs, but not in CD133(-) cells.

(**D**) qRT-PCR analysis of NANOG target genes in the presence or absence of NANOG or STAT3. TICs were transduced, as indicated, by lentivirus overexpressing *Nanog* (OE), shRNA targeting *Nanog* (sh-*Nanog*), retrovirus expressing dominant negative form of STAT3 (STAT3D) or constitutively active form of STAT3 (STAT3C). qRT-PCR analysis of NANOG target genes were performed. All experiments were conducted with TICs. *P* values represent two-tailed Student's *t*-tests between untransduced and transduced cells. Values for each cell line are means ± S.D., n=4, **P*<0.01, ***P*<0.001. Values for each cell line are means ± S.D., n=4.

(**E**) *De novo* Nanog-binding motifs resemble STAT3-binding motifs.

(**F**) Silencing *Nanog* reduces STAT3-mediated transactivation in TICs. **P*<0.01, ***P*<0.001, n=4.

Figure S1
Chen *et al.*

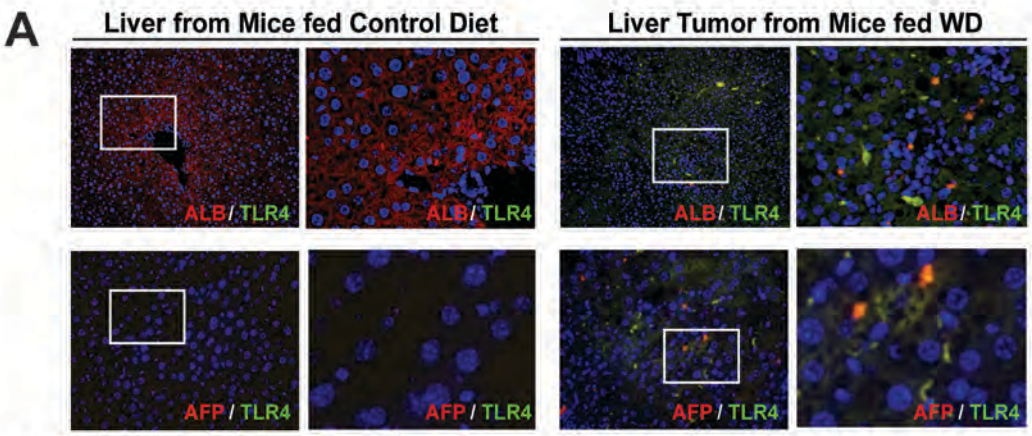

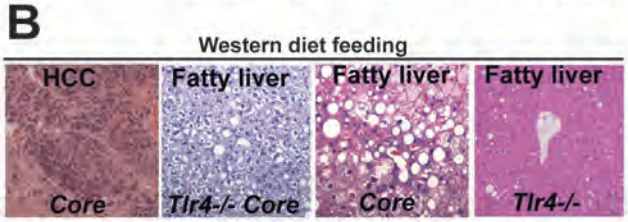

Histology	WT Dysplastic nodule	WT HCC	*Core* Dysplastic nodule	*Core* HCC
Control diet	1/20 (0%)	0/20 (0%)	1/22 (4.6%)	1/22 (4.6%)
Ethanol diet	0/36 (0%)	0/36 (0%)	8/19 (25.8%)	4/19 (12.9%)
Lean fat diet	1/25 (4%)	0/25 (0%)	1/19 (5.3%)	1/19 (5.3%)
Western diet	2/32 (6.3%)	0/32 (0%)	4/21 (19.1%)	4/21 (19.1%)

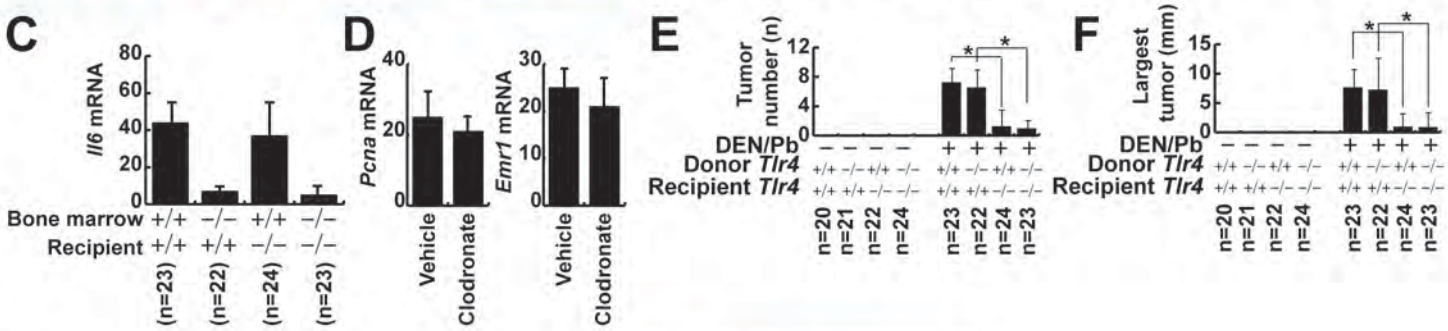

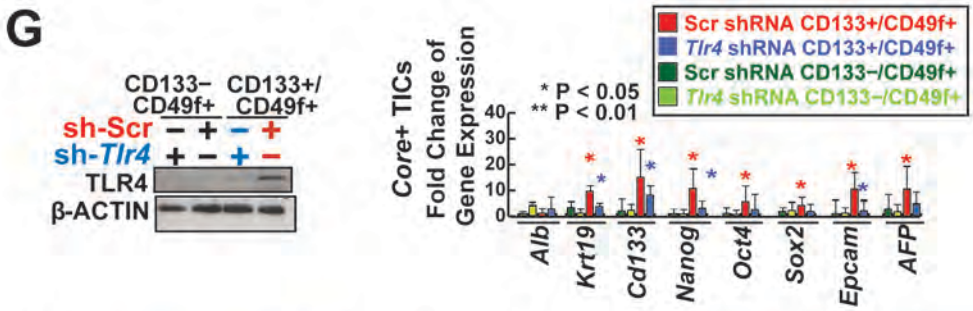

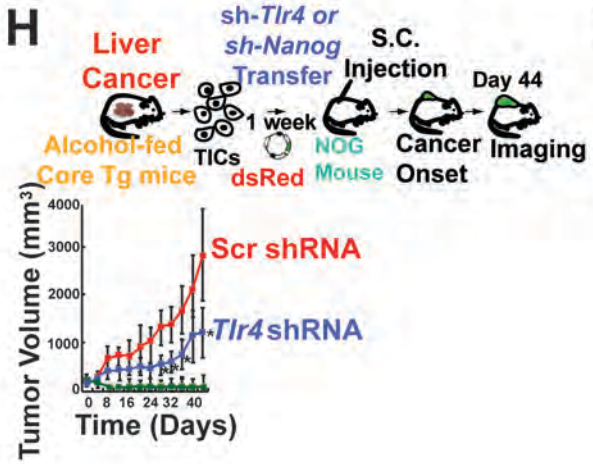

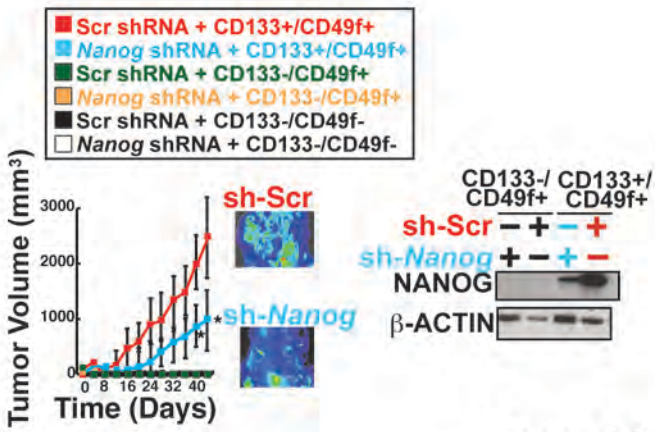

Figure S2 Continued
Chen *et al.*

Fig. S2 (related to Fig. 2). Validation of reconstituted bone-marrow-derived cells and Tlr4- and Nanog-dependency of mouse TICs isolated from liver tumor model.

(**A**) Immunostaining of liver sections of Western diet-fed mice. Immunofluorescence staining of Albumin (ALB), α-Fetoprotein (AFP) and TLR4 in liver sections from Western diet (WD)-fed mice.

(**B, left**) Liver histology and tumor incidence of WD fed HCV-Core and HCV-*Core/Tlr4*(-/-) Tg mice. Upper panel (left to right)-representative H&E stained liver sections from HCC-*Core*, typical examples of fatty liver, and *Tlr4*-/- mice fed high fat diet. Nodular lesions differ from the surrounding liver parenchyma with cytological or structural atypia. (**B, right**) Frequencies of liver dysplastic nodules and HCCs in WT or *Core* Tg mice fed control diet or Western diet (WD) for 12 months. The histopathology of the tumors (arrows) shown are dysplastic nodules (DNs) or hepatocellular carcinomas (HCCs) based on their hypercellularity.

(**C**) Validation of efficiency of reconstitution of bone marrow transplantation. Efficiency of reconstitution of bone marrow transplantation was confirmed by LPS-induced *Il6* mRNA expression in isolated splenocytes from TLR4-chimeric mice in comparison to that of untreated mice.

(**D**) WT mice were treated with DEN followed by liposomal clodronate injection (n=18) or liposome vehicle injection (n=12) before phenobarbital feeding. Marker of Kupffer cell (liver-resident macrophage: *Emr1*) depletion and proliferation marker (*Pcna*) were evaluated by qPCR.

(**E** and **F**) Tumor number and size of *Tlr4* WT (+/+) or deficient (–/–) mice with bone marrow transplantation of WT or *Tlr4* deficient cells injected with DEN and fed phenobarbital (Pb)-containing water.

(**G**) We performed FACS-based isolation of CD133+/CD49f+ cells from liver tumors of alcohol-fed Core Tg mice. CD133+/CD49f+ cells from these models all have higher expression of stemness genes such as *Cd133*, *Nanog*, *Oct4*, and *Sox2* compared to CD133- cells, and the inductions are abrogated by Tlr4 silencing with lentiviral shRNA. CD133+/CD49f+ cells from the three HCC models, express stemness genes.

(**H** and **I**) CD133+/CD49f+ cells form tumors in NOG mice in a manner dependent on TLR4 or NANOG. CD133+/CD49f+ TICs isolated from human HCC have tumorigenic activities dependent on TLR4 and NANOG. Scr: Scrambled shRNA-transduced cells. Tumor-initiation property is increased in CD133+ cells and suppressed by *Tlr4* (**H**) or *Nanog* (**I**) silencing, demonstrating they are self-renewing. Subcutaneous transplantation of CD133+ cells but not CD133- cells transduced with a dsRed lentiviral vector, results in tumor formation in immunocompromised NOG mice, and the tumor growth assessed by dsRed imaging is attenuated by *Tlr4* or *Nanog* silencing with lentiviral shRNA prior to transplantation. These results are supportive that CD133+/CD49f+ cells are TLR4/NANOG-dependent TICs and that *Tlr4* is a putative proto-oncogene involved in the genesis of TICs.

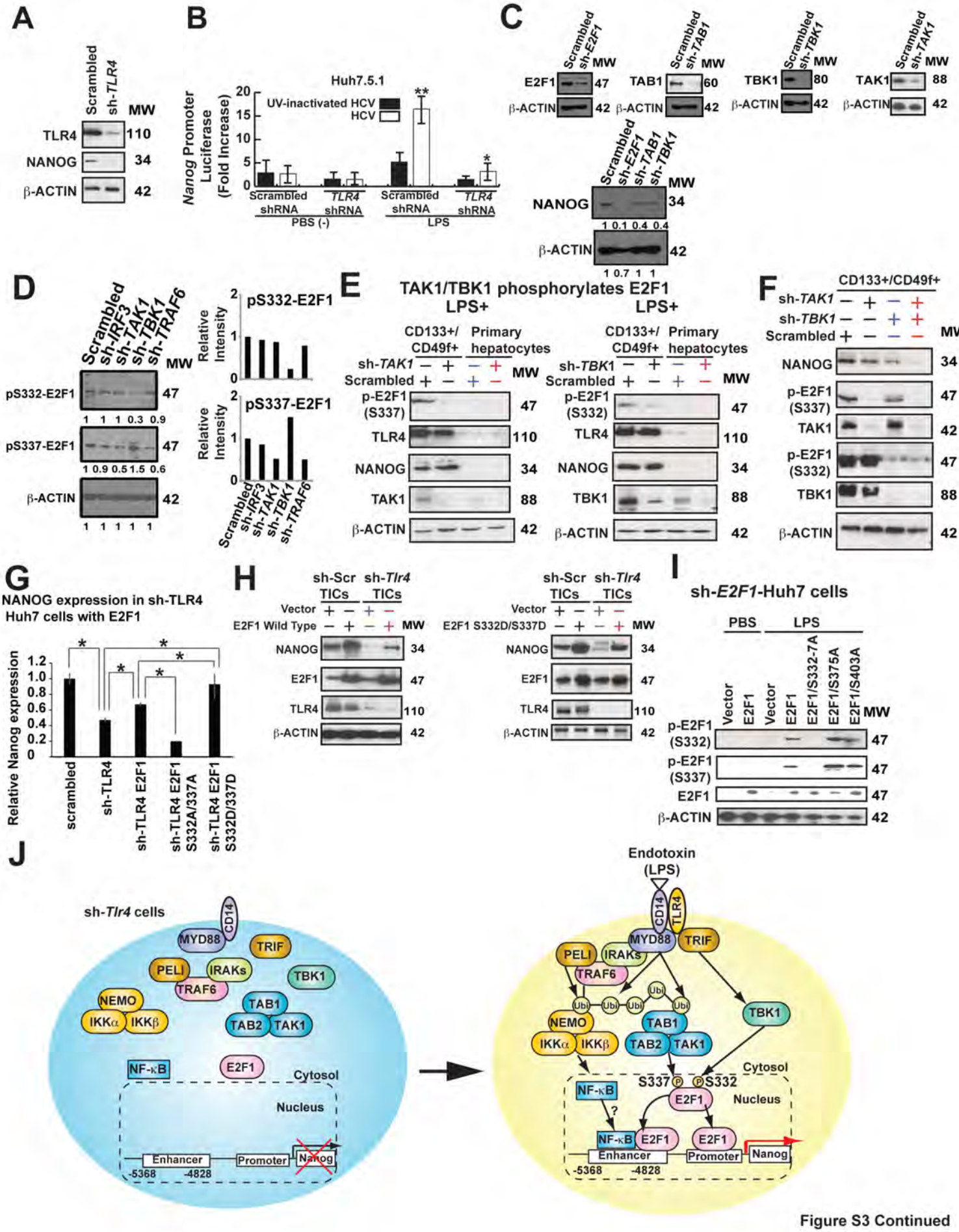

Figure S3 Continued
Chen *et al.*

Fig. S3 (Related to Fig. 3). TLR4 stimulation transactivates NANOG through TAK1 and TBK1-mediated phosphorylation of E2F1 at serines 337 and 332.

(**A**) TLR4 silencing effect was confirmed by immunoblot in Huh7.5.1 cells.

(**B**) Role of TLR4 activation of *Nanog* promoter in human hepatocytes with HCV infection. HCV infection in Huh7.5.1 cells induced NANOG promoter activity in response to LPS stimulation. LPS transactivates Nanog through TLR4 signaling. All experiments were conducted with Huh7.5.1 cells. *P* values represent two-tailed Student's *t*-tests between untransduced and transduced cells. Values for each cell line are means ± S.D., n=4, **P*<0.01, ***P*<0.001.

(**C**) Silencing of E2F1, TAB1 (TAK1-binding protein: MAP3K7), TBK1 or TAK1 was confirmed by immunoblots. Silencing E2F1, TAB1 or TBK1 reduces NANOG protein levels in TICs.

(**D**) TLR4-mediated TAK1/TBK1 phosphorylation of E2F1 transactivated NANOG promoter in TICs. (**D**, right) Densitometric analysis of immunoblots bands.

(**E**) TAK1 and TBK1 were required for efficient transactivation via E2F1 phosphorylation. Several shRNAs targeting E2F1-tranduced TICs were transfected with WT E2F1, E2F1(Ser332Ala), E2F1(Ser337Ala) and E2F1(Ser332Ala, Ser337Ala) and stimulated for LPS.

(**F**) Silencing both TAK1 and TBK1 reduced E2F1 phosphorylation at two serine residues (Ser332 and Ser337) and reduced NANOG protein levels after LPS stimulation.

(**G**) Non-phosphorylatable mutant of E2F1 does not induce NANOG expression in TLR-silenced Huh7 cells.

(**H**) Expression of E2F1 (S332D/S337D) in Tlr4-silenced TICs promoted NANOG protein expression.

(**I**) Alanine substitution of phosphorylation sites (aa332-337) abrogated phosphorylation of S332 and S337 following LPS stimulation. Several shRNAs targeting E2F1-tranduced TICs were transfected with WT E2F1, E2F1(Ser332Ala), E2F1(Ser337Ala) and E2F1(Ser332Ala, Ser337Ala) and stimulated by LPS.

(**J**) Proposed model. Schematic indicates the predicted elements within the Nanog enhancer and promoter. Phosphorylation of E2F1 and/or overexpression of E2F1 may activate *Nanog* transcription at the enhancer and promoter.

Figure S3
Chen *et al.*

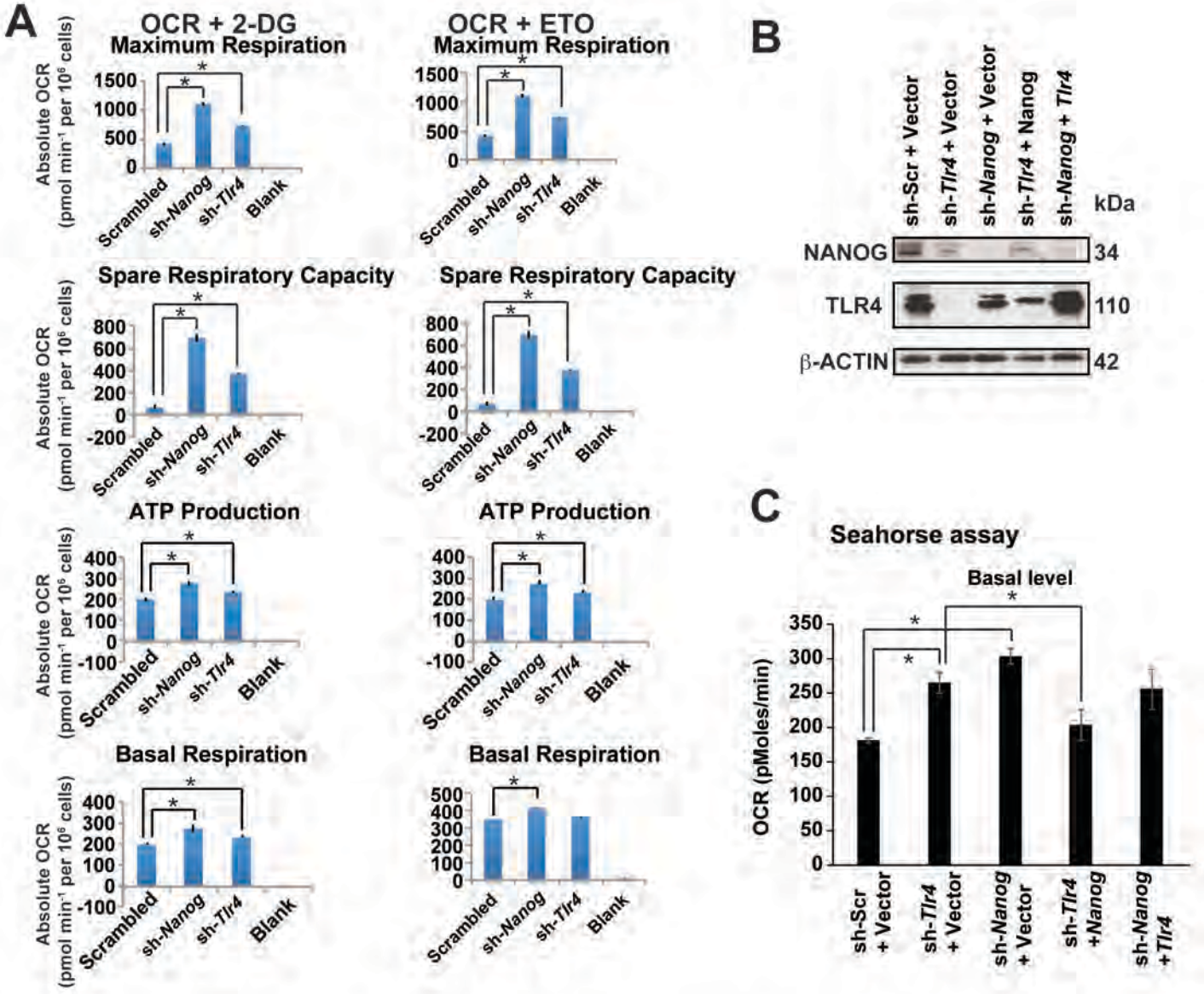

Fig. S4 (Related to Fig. 4). Silencing of Tlr4 or Nanog promotes basal levels of oxygen consumption rate.

(**A**) Maximum respiratory capacity, spare respiratory capacity, ATP production and basal respiration in sh-*Nanog*, sh-*Tlr4* and sh-Scrambled TICs. **P*<0.05.

(**B**) Protein levels of NANOG and TLR4 were confirmed in sh-Scrambled, sh-*Nanog* or sh-*Tlr4* TICs in the presence or absence of overexpression of NANOG or TLR4.

(**C**) NANOG overexpression restored lower levels of basal respiration in sh-Tlr4-TICs while TLR4 overexpression did not return to basal level of OCR in sh-Nanog-TICs. Seahorse assays using sh-*Tlr4* or sh-*Nanog* lentivirus-transduced TICs in the presence or absence of Nanog or TLR4 overexpression, respectively. NANOG overexpression in sh-*Tlr4*-TICs reduced OCR to a similar level as for sh-Scrambled-TICs. In contrast, overexpression of TLR4 in sh-*Nanog*-TICs did not reduce OCR at the level of sh-Scrambled TICs, indicating that TLR4-mediated NANOG induction mainly reduced OXPHOS (i.e., OCR levels) in TICs. **P*<0.05.

Figure S4
Chen *et al.*

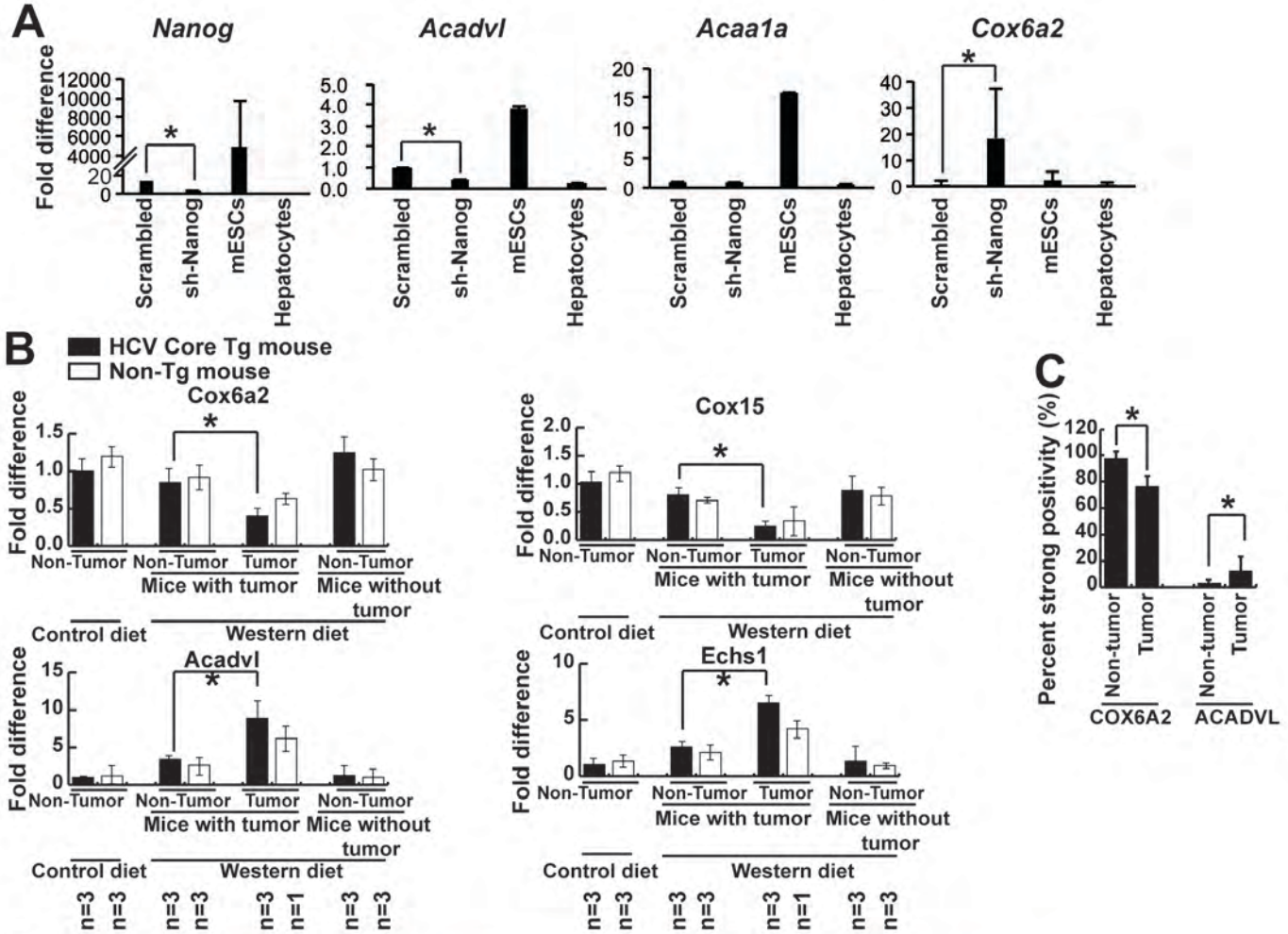

Figure S5 Continued
Chen *et al.*

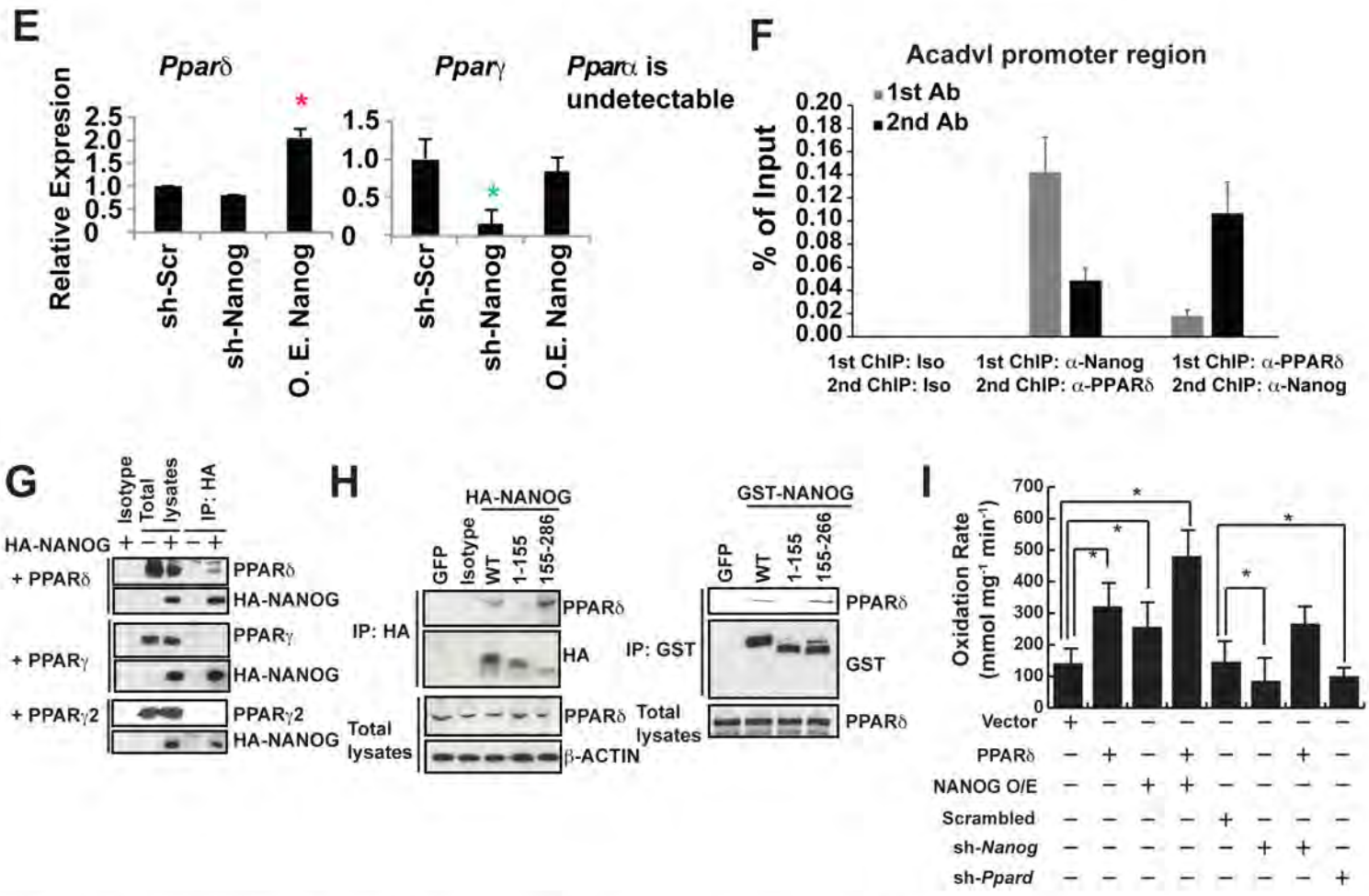

Fig. S5 (Related to Fig. 5). NANOG cooperates PPARs to promote FAO of TICs.

(**A**) qRT-PCR analysis of peroxisomal and mitochondrial FAO gene expression in mouse ESCs, primary hepatocytes or mouse TICs transduced with scramled shRNA or sh-Nanog. Peroxisomal FAO gene Acaa1 (one of Nanog target gene) is not altered by Nanog silencing in TICs.

(**B-D**) Tumor-bearing mice have higher level of FAO genes, but lower levels of OXPHOS-related genes while mice without tumors have similar gene expression profile with those of non-tumor part of livers. (**B**) qRT-PCR in mouse tissues. n: numbers of liver specimens analyzed by qRT-PCR. (Note: due to lower tumor incidence of non-Tg mice fed Western diet (WD), the sample number was only one. (**C**) Staining data quantified by blind analysis by two board-certified pathologists. (**D**) Immunohistochemistry of mouse tissues.

(**E**) qRT-PCR analysis of *PPAR* mRNA levels in sh-Scr-TICs or TICs with shRNA targeting of Nanog (sh-*Nanog*) or overexpression (O.E.) of Nanog.

(**F**) Sequential ChIP-qPCR analysis of Acadvl promoter region.

(**G-H**) PPARδ physically interacted with NANOG. TICs co-transfected with PPARs and HA-tagged Nanog wild-type or the deletion mutants were lysed, immunoprecipitated by α-HA antibody and assayed by immunoblotting with indicated antibodies. Western blots of total lysates or proteins immunoprecipitated with an anti-HA (IP HA) antibody were probed with antibodies.

(**H**) Lysates of TICs transfected with HA or the indicated GST-tagged *Nanog* deletions were incubated to capture with HA-Sepharose or Glutathione–Sepharose.

(**I**) PPARδ promotes FAO. Fatty acid oxidation rate was measured in the presence or absence of NANOG overexpression or PPARδ.

Figure S5
Chen *et al.*

A Culture Media of sh-Nanog-TICs vs.Scr-TICs

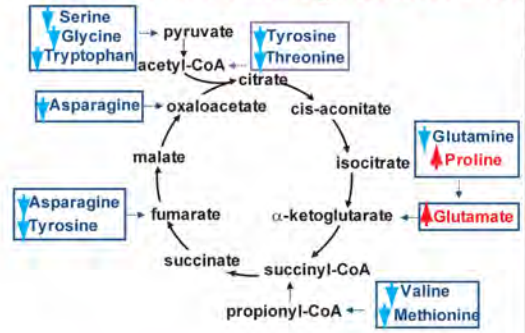

Sub Pathway	Biochemical Name	Fold Change CD133(-) sh-Nanog / Scr	Fold Change TICs sh-Nanog / Scr
Amino acids	glycine	1.22	0.76
	serine	1.14	0.65
	threonine	0.85	0.88
	alanine	1.27	1.41
	aspartate	1.27	0.99
	asparagine	1	0.5
	glutamate	1.16	1.44
	glutamine	0.79	0.56
	histidine	1.07	0.75
	lysine	1.03	0.78
	phenylalanine	1.1	0.81
	tyrosine	1.03	0.8
	tryptophan	1.07	0.49
	leucine	1.06	0.71
	isoleucine	1.01	0.86
	valine	1.01	0.79
	methionine	1.01	0.51
	cysteine	1.13	1.18
	arginine	1	0.93
	proline	1.13	1.2

B Culture Cells of TICs vs. CD133(-) cells

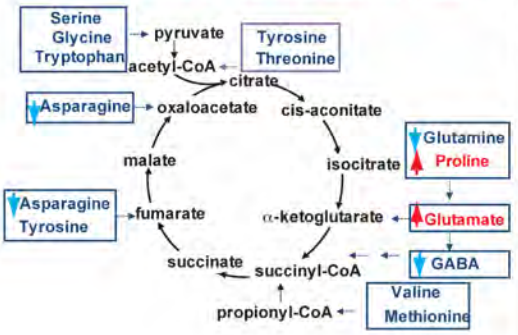

Sub Pathway	Biochemical Name	Fold Change TICs / CD133(-)
Amino acids	glycine	0.97
	serine	0.66
	threonine	0.57
	alanine	0.96
	aspartate	2.53
	asparagine	0.28
	glutamate	5.14
	glutamine	0.3
	histidine	0.86
	lysine	0.92
	phenylalanine	0.83
	tyrosine	0.79
	tryptophan	0.96
	leucine	0.88
	isoleucine	0.83
	valine	0.75
	methionine	0.91
	cysteine	0.26
	arginine	2.06
	proline	4.81
Glutamate	gamma-aminobutyrate (GABA)	0.33
	glutamate, gamma-methyl ester	22.47

C Metabolites in cells

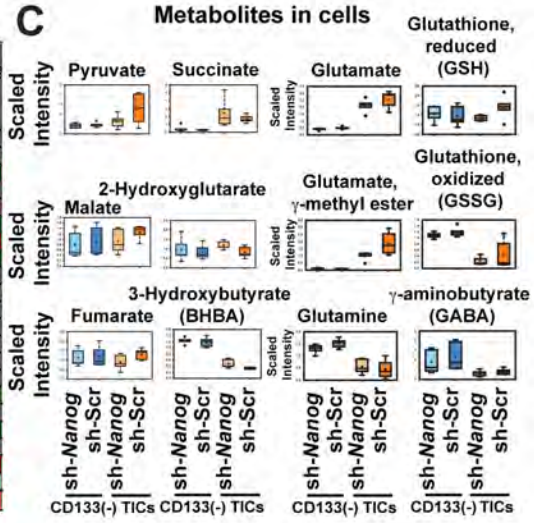

D

E

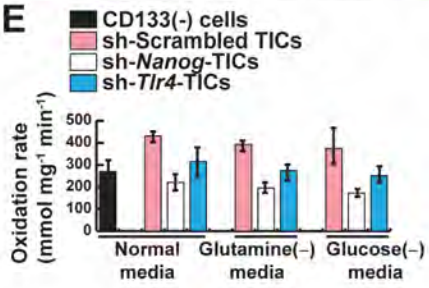

F

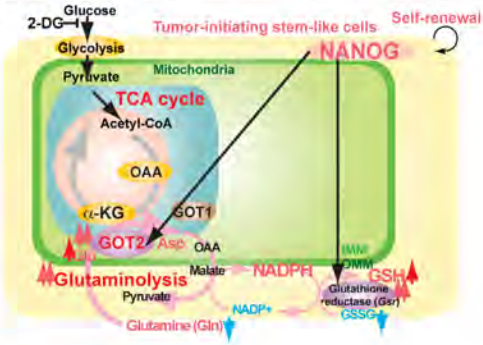

G

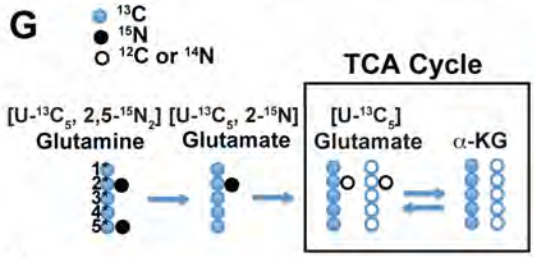

C2-C4 Fragment

	M0	M1	M2	M3	M4
Scrambled	20.4	22.5	19.3	23.8	14.1
sh-*TLR4*	27.7	24.4	17.5	18.9	11.4
sh-*Nanog*	25.9	25.7	17.7	19.0	10.7
Scrambled Vigabatrin	18.7	22.4	18.6	24.9	15.4
sh-*TLR4* Vigabatrin	25.9	24.4	17.4	20.5	11.8
sh-*Nanog* Vigabatrin	25.1	26.5	18.0	20.1	10.3

H Culture Cells of sh-*Nanog* TICs vs. Scr-TICs

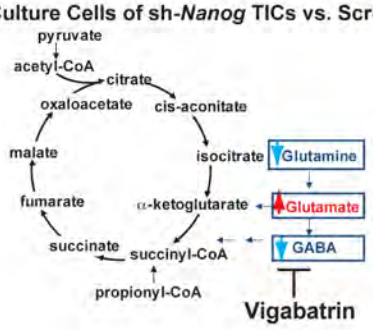

C2-C5 Fragment

	M0	M1	M2	M3	M4	M5
Scrambled	18.4	21.7	18.8	10.4	15.6	15.1
sh-*TLR4*	26.1	23.5	17.0	8.2	12.7	12.4
sh-*Nanog*	25.0	24.4	17.5	8.3	13.4	11.4
Scrambled Vigabatrin	18.3	21.2	18.0	10.3	15.9	16.3
sh-*TLR4* Vigabatrin	24.4	23.5	17.2	8.5	13.6	12.7
sh-*Nanog* Vigabatrin	25.7	25.5	17.6	8.2	12.6	10.4

M0: unlabeled glutamate
M1-M4: labeled glutamate in TCA cycle
M5: labeled glutamate derived from [U-$^{13}C_5$, 2,5-$^{15}N_2$]-glutamine

Figure S6 Continued
Chen *et al.*

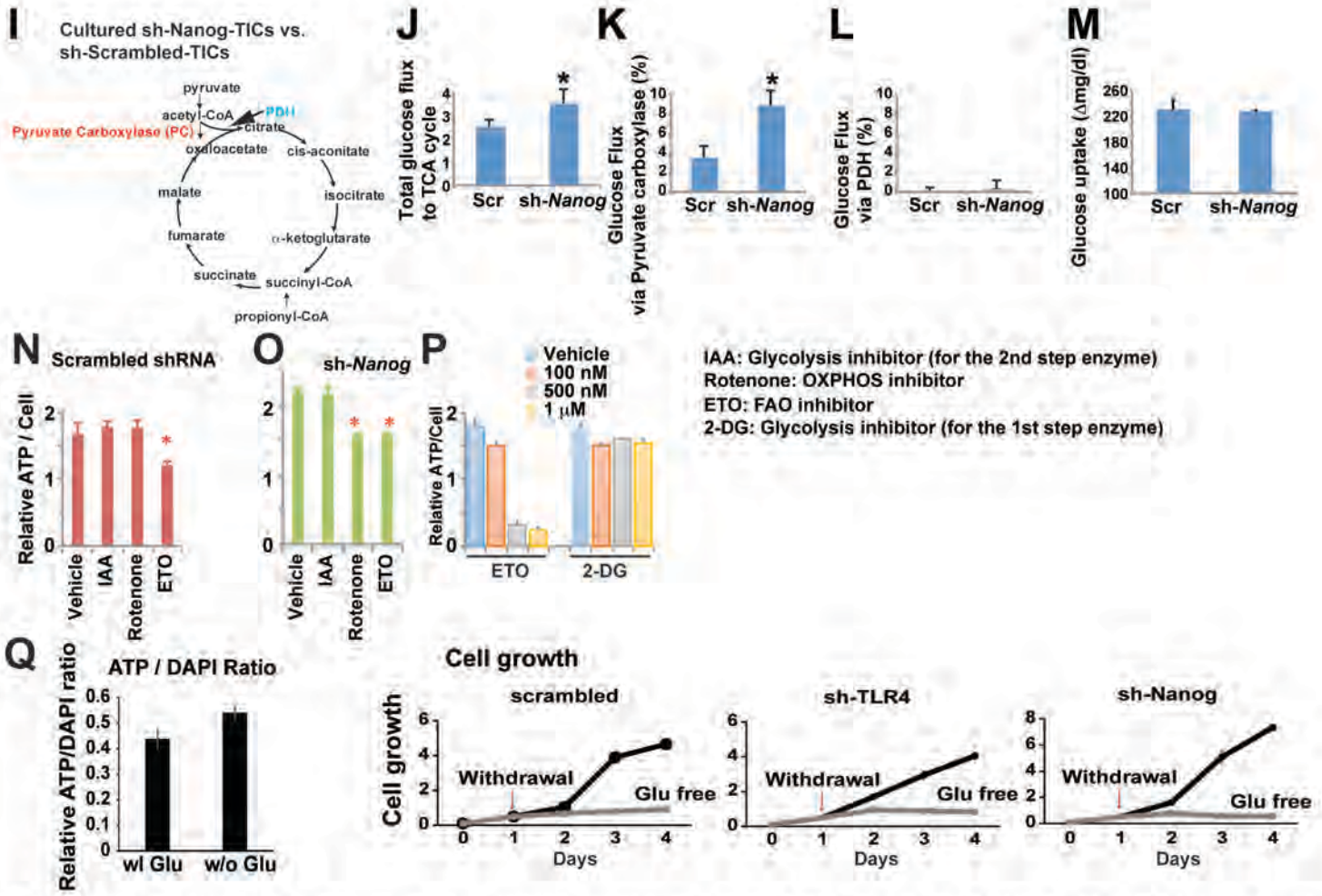

Fig. S6 Continued (Related to Fig. 6) Siilencing Nanog promotes glutaminolysis pathway, ATP production and glucose flux in TICs judged by metabolomics analysis, qRT-PCR and stable istope experiments.

(**A**) Glutaminolysis pathway in TICs judged by metabolomics analysis. Amino acid levels by metabolomic analysis of media from CD133(-) and TICs transduced with scrambled shRNA or sh-*Nanog*. (**A, right**) (**C**) Representative metabolites of cells from metabolomics analyses.

(**B**) Amino acid levels following metabolomic analysis of cells from CD133(-) and TICs transduced with scrambled shRNA or sh-*Nanog*.

(**C**) Representative metabolites of cells from metabolomics analyses. (**D-F**) Glutaminolysis pathway in TICs judged by qRT-PCR and FAO analysis.

(**D**) qRT-PCR analysis of *Got2* and Glutathione reductase (*Grs*) in TICs transduced with Nanog, scrambled shRNA or sh-*Nanog* lentivirus.

(**E**) Oxidation rate was measured in TICs transduced with lentivirus sh-*Tlr4*, sh-*Nanog* or sh-Scrambled in glucose-deficient (–), glutamine-deficient (–) or normal culture media.

(**F**) NANOG-mediated glutaminolysis induces generation of antioxidant molecules, including glutathione (GSH) through activation of glutaminolysis-related enzymes, including GOT2 and Glutathione reductase (*Gsr*).

(**G**) C2-C4 fragment relative abundance of glutamate (%) in TICs. M0, unlabeled glutamate; M1-M3, labeled glutamate in TCA cycle; M4, labeled glutamate derived from [U-$^{13}C_5$, 2,5-$^{15}N_2$]-glutamine taken up the cells. When [U-$^{13}C_5$, 2,5-$^{15}N_2$]-glutamine is taken up by cells, it loses the ^{15}N on the 5th carbon and is converted to [U-$^{13}C_5$, 2-^{15}N]-glutamate, which loses the ^{15}N on the 2nd carbon and becomes [U-$^{13}C_5$]-glutamate after rapid equilibration with TCA cycle intermediate α-ketoglutarate. When glutamine and glutamate are analyzed by gas chromatography mass spectrometry under electronic impact ionization (EI), their TFA derivatives give rise to a C2-C4 (m/z 152) and C2-C5 (m/z 198) fragments (Lee, 1996). Thus, the [U-$^{13}C_5$, 2-^{15}N]-glutamate has a C2-C4 fragment of m/z 156 (M4; contains 3x^{13}C and a ^{15}N) and a C2-C5 fragment of m/z 204 (M5; contains 4x^{13}C and a ^{15}N), which represent the relative abundance of glutamine taken up by the TICs. On the other hand, [U-$^{13}C_5$]-glutamate has a C2-C4 fragment of m/z 155 (M3; contains 3x^{13}C) and a C2-C5 fragment of m/z 204 (M4; contains 4x^{13}C). When the [U-$^{13}C_5$]-glutamate enters TCA cycle metabolism, it will gradually lose the ^{13}C carbon after each cycle to generate M2, M1, and M0 C2-C4 fragment and M3, M2, M1, and M0 C2-C5 fragments, which represent the TCA cycle activity (Lee, 1996).

(**H**) Relative abundance of glutamate (%) in TICs. As shown in the table above sh-*TLR4* or sh-*Nanog* silencing reduced glutamine uptake by the TICs as evident by decreased percentage of M3 and M4 glutamate (C2-C4) and M4 and M5 (C2-C5) fragments. However, sh-*Tlr4* or sh-*Nanog* silencing enhances TCA cycle activity as demonstrated by the increased generation of M0 and M1 glutamate in both fragments. Treatment of TICs with the irreversible inhibitor of the key 'GABA shunt' enzyme GABA transaminase, vigabatrin, does not reduce the percentage of labelled succinate, suggesting that sh-*Tlr4* or sh-*Nanog* silencing promotes glutamine oxidation in mitochondria.

(**I**) TCA cycle of sh-Nanog TICs when compared to sh-Scrambled TICs.

(**J-M**) Carbon flux analysis demonstrates that Nanog silencing induces glucose flux through pyruvate carboxylase, but not PDH pathway. Glucose flux analysis. There is a slight increase in total glucose flux to TCA after *Nanog* silencing. (**K**) *Nanog* silencing results in >5% flux through PC, comparing to Scrambled TICs (sh-Scr-TICs) group. (**L**) In both Scrambled shRNA (sh-Scr) and *Nanong* silencing TICs (sh-*Nanog*-TICs) groups, glucose flux through PDH for oxidation is negligible. (**M**) Glucose uptake was not significantly changed.

(**N** and **O**) ATP production is reduced in ETO-treated TICs. Relative ATP levels per cell were plotted in TICs transduced with (**N**) scrambled shRNA or (**O**) sh-*Nanog*.

(**P**) ETO treatment reduced ATP production while glycolysis inhibitor (2-DG) does not significantly lower ATP production in TICs.

(**Q**) Glutamine withdrawal did not significantly change ATP production (**Left**), but reduced cell growth rate in all TICs in the presence or absence of silencing of TLR4 or NANOG (**Right**).

Figure S6
Chen *et al.*

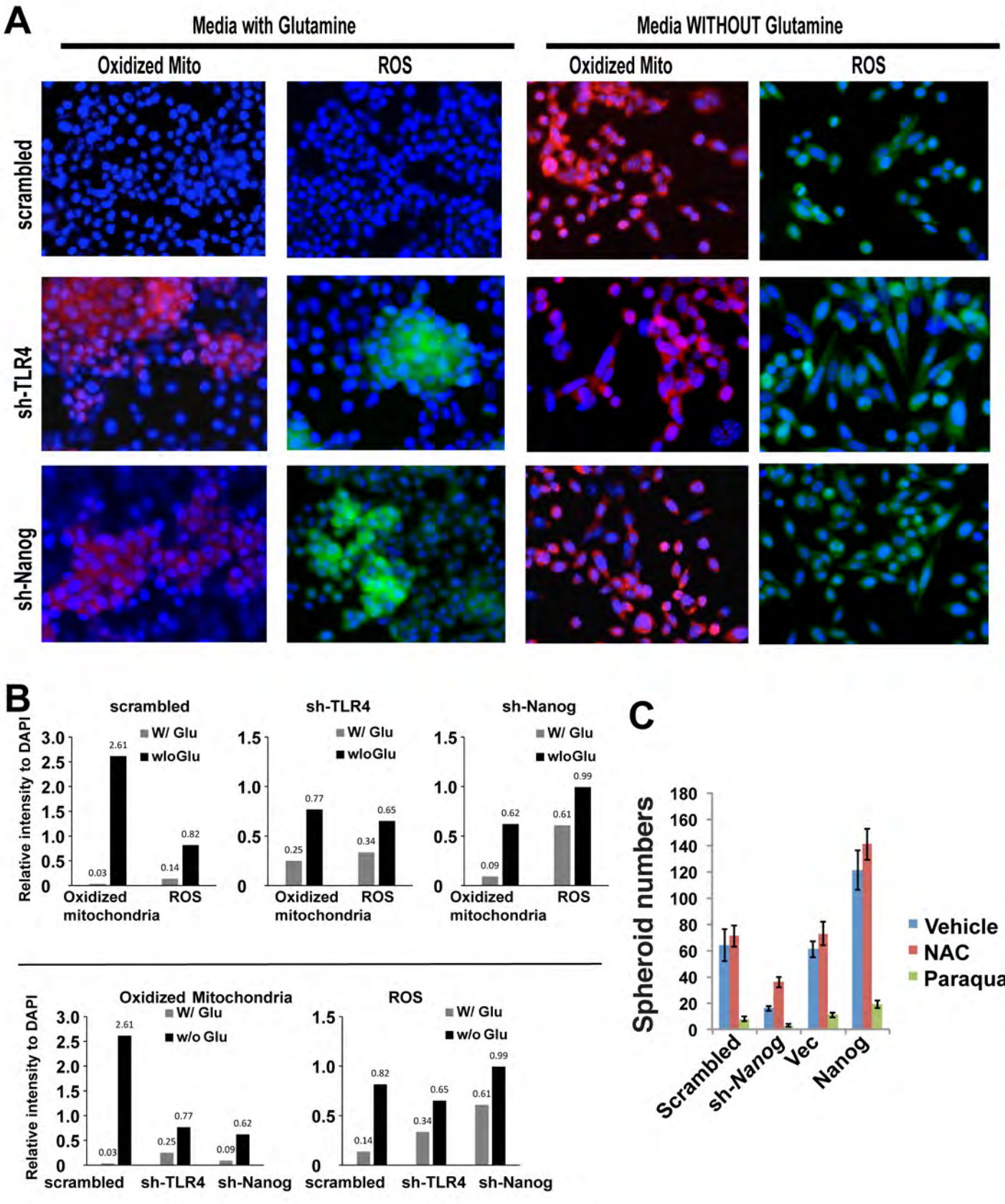

Figure S7 Continued
Chen *et al.*

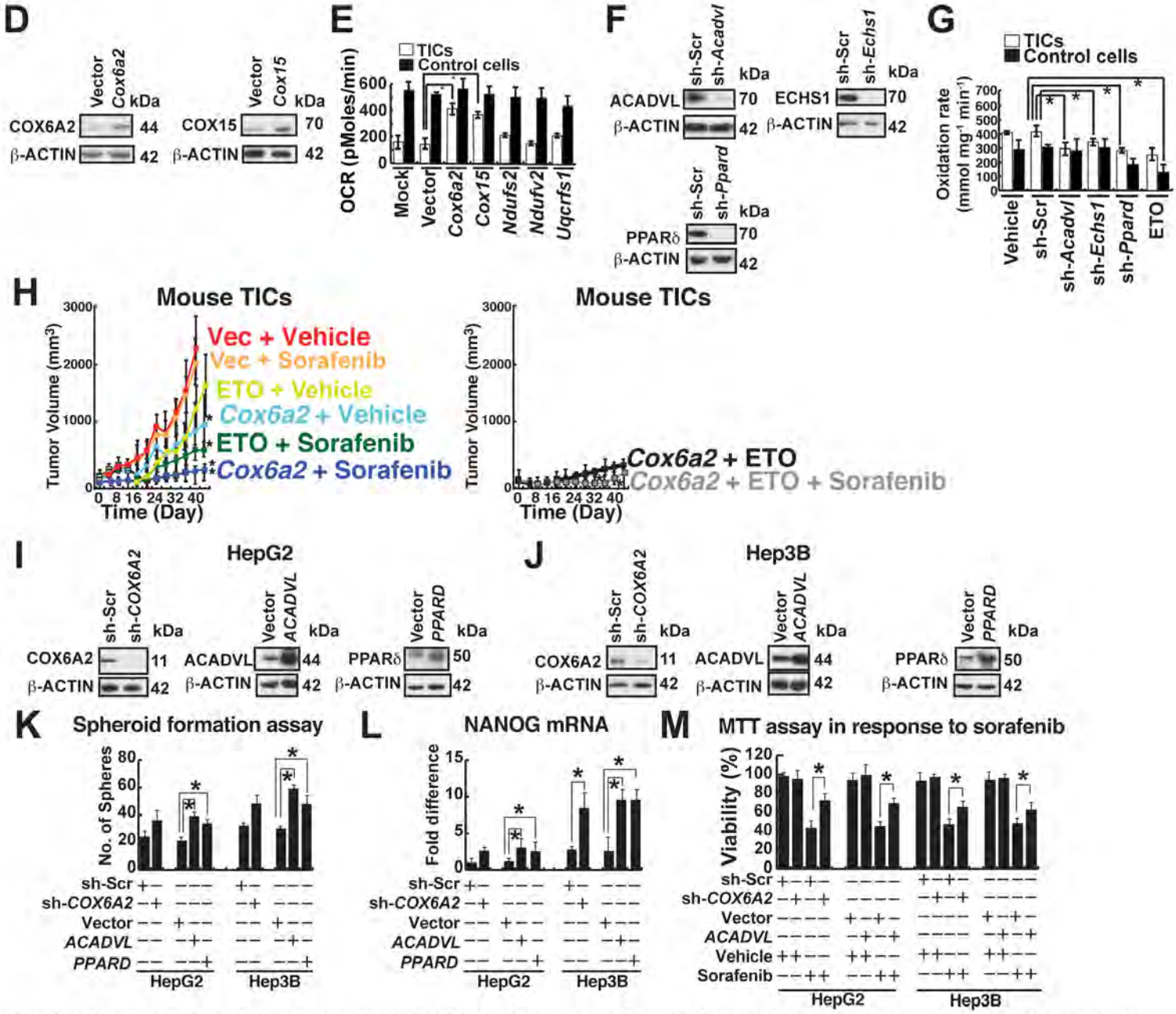

Fig. S7 (Related to Fig. 7). Restoration of OXPHOS and/or suppression of FAO reduce the tumor growth and drug resistance. (**A-B**) **ROS production is increased by glutamine removal in TICs regardless of silencing of Nanog or Tlr4.** (**A**) Glutamine withdrawal induced ROS production in all TICs in the presence or absence of silencing of TLR4 or NANOG. (**B**) Quantified data are plotted.

(**C**) *Nanog* silencing reduced spheroid formation through ROS production in TICs.

(**D-H**) NANOG orchestrates in TICs the oncogenic and therapeutic resistant mechanisms that result from mitochondrial metabolic reprogramming. (**D**) Overexpression of Cox6a2 or Cox15 were confirmed by immunoblots. (**E**) Restoration of OXPHOS genes (*COX-6A2* and *COX15*) in TICs promoted OCR (**E**). (**F**) Silencing effects of shRNA targeting Acadvl or Echs1 were confirmed by immunoblots. (**G**) Silencing *Acadvl* and *Echs1* reduced rate of FAO. (**H**) Correlation of NANOG-mediated suppression of FAO and role in tumor formation. Mouse TICs were transduced with lentiviral *Cox6a2* gene and were subcutaneously transplanted into NOG mice. These mouse TICs were very resistant to the growth inhibitory effect of sorafenib. By contrast expression of Cox6a2 abrogated this resistance and reduced tumor growth in comparison to vehicle treatment alone or control vector group. This demonstrated that overexpression of OXPHOS gene (*Cox6a2*) and inhibition of FAO by blocking entry of fatty acids into mitochondria (ETO) sensitized TICs to sorafenib and inhibited xenograft tumor growth engrafted with mouse TICs in mouse recipients.

(**I-M**) *COX6A2* silencing or *ACADVL* overexpression promoted self-renewal ability and NANOG expression in human HCC cell lines.

(**I** and **J**) Silencing of COX6A2 proteins with shRNA lentivirus transduction or overexpression of ACADVL or PPARD was confirmed by immunoblot analysis (**I:** HepG2 and **J:** Hep3B).

(**K** and **L**) Reduction of OXPHOS gene (e.g., *COX6A2*) or overexpression of FAO gene (e.g., *ACADVL*) in human non-TIC HCC cell lines (HepG2 and Hep3B) promoted self-renewal ability (**K**), NANOG expression (**L**) and viability in response to sorafenib treatment (**M**), as judged by spheroid formation assays, qRT-PCR analysis of NANOG and MTT staining assays respectively following sorafenib treatment (10 μM, 48 hours).

Figure S7
Chen *et al.*

Supplemental Experimental Procedures

Cell lines

TICs were grown in DMEM/F12 or Kubota medium for all experiments. HEK293T and Huh7 cells were cultured in DMEM (Cellgro) with 10% FBS and essential amino acid supplements.

Vector

PPARδ expression and mutant (1-299 aa truncation form) constructs are gifts from Dr. Carlo V. Catapano at the Oncology Institute of Southern Switzerland.

Endotoxin measurement

For endotoxin measurements, blood was collected from inferior vena cava with pyrogen-free heparin as previously described (Mathurin et al., 2000)). Extreme care was taken to eliminate pyrogen and endotoxin contamination of all surgical instruments and laboratory supplies. Blood samples were transferred to appropriate glass tubes made pyrogen-free by heating at 180°C for 24 hr. Pyrogen-free water was supplied by the manufacturer. Immediately before assay, plasma samples were diluted and heated to 75°C for 10 minutes to denature endotoxin-binding proteins that can mask endotoxin detection. Levels of endotoxin were measured using the Limulus amebocyte lysate pyrogen test and a kinetic assay program (Kinetic test, Kinetic-QCL, Santa Clara, CA; BioWhittaker). The threshold of endotoxin detection was 0.1 pg/mL.

dsRed imaging analysis

Tumor progression and metastases (in lungs and spleens) were monitored by whole-body dsRed bioluminescence imaging (IVIS system, Xenogen) every 8 days over 90 days, as previously described. Images were captured directly to a microcomputer (Xenogen). Imaging at lower magnification that visualizes the entire animal were carried out in a light box illuminated by blue light fiber optics (Xenogen, Inc.), and images were recorded with a thermoelectrically cooled color CCD camera.

Tumor collection and analysis

Harvested tumors were measured for the actual volume and weight. The tumor tissues were divided for snap-freezing for mRNA and protein analysis of targeted OXPHOS/FAO genes and histological fixation with 3% paraformaldehyde followed by sucrose treatment for subsequent immune-staining and target gene products.

Gene array analysis of liver

Systematic gene microarray analyses were performed for dysplastic and normal tumors, to identify changes in known or unknown signaling pathways that are tightly associated with synergistic induction of liver tumor by Western diet (WD) or alcohol. For microarray analysis, livers isolated from five mice were subjected to RNA isolation, later pooled to achieve collection of sufficient amounts of samples for hybridization to the mouse microarray (Affymetrix Inc.). The Affymetrix mouse gene chip (Mouse genome 430.2 array) was used and hybridization and scanning was in the Genome Core Facility Children's Hospital, Los Angeles. Genes were categorized by related functions for assessment of pathophysiological effects of alcohol in liver. 83 gene transcripts of those positive showed increased expression using 4.0 fold (balanced differential expression) as a cutoff. To identify changes associated with synergism by alcohol or WD, comparative analysis was done in the cells isolated from non-Tg mice vs. Tg mice fed WD. Briefly, data was background-corrected normalized by RMA (Robust multi-array average) and transformed to median of control samples. Probe level data was summarized to gene

level. To find differentially expressed genes a t-test ($p<0.05$) was used and genes were further ranked by a fold change. The data has been deposited in GEO of NCBI under GSE.

Proteomics

Proteomic analysis was performed at the Proteomic Exploration Laboratory at California Institute of Technology, Pasadena, CA. In brief, the livers were lysed for protein extraction and extracted proteins were subjected to one-dimensional gel electrophoresis, and stained protein bands were used for in-gel trypsin digestion and MS sequencing.

Chemicals and reagents. Trypsin (modified sequencing grade) was from Promega (Madison, WI). Acetonitrile and water (Chromasolv LC-MS quality), iodoacetamide (99+%), trifluoroacetic acid (99+%), dithiothreitol (DTT 99%) and glacial acetic acid (99%) were supplied by Sigma-Aldrich (St. Louis, MO).

Isolation and preparation of proteins from mouse liver. Animal handling followed AALAC and National Institutes of Health guidelines, and experimental procedures were approved by the IACUC. Tissues were homogenized in 1 ml of sodium phosphate buffer (pH 7.4) using Polytron homogenizer at 4°C. Low speed centrifuge (800 rpm) was used to remove non-homgenized tissues and debris. Supernatants were centrifuged and 0.136 ml of 80% sucrose was added to 1 ml of sample. Sodium phosphate buffer (pH 7.4 with protease inhibitor) was added, centrifuged for 1 hr at 4°C at 35,000 rpm and washed three times with Tris-EDTA (10 mM Tris, 1 mM EDTA) buffer. Pellet fraction was subjected to chloroform, methanol and water extraction. The proteins (the interface) were collected and were centrifuged for 15 min at 10,000 rpm. The pellet was washed using Tris-EDTA buffer.

Separation of proteins by 1D PAGE. The protein (10-50 µg in 20 µL of LDS sample buffer) were separated using 1D SDS PAGE on a 10% BisTris NuPAGE gel using NuPAGE MES SDS running buffer (20X) at a voltage of 120V for the first half hour after which the voltage was reduced to 80V The separated proteins on the gel were stained using colloidal Coomassie blue (Invitrogen, Carlsbad, CA).

Protein in-gel digestion. The proteins on the gel were sectioned into 20 pieces, minced and destained using 50 mM ammonium bicarbonate buffer (pH 8.0) and acetonitrile. The proteins were reduced with 25 µl of 10 mM DTT and alkylated using 25 µl of 55 mM iodoacetamide. The proteins were digested using 25 µl of trypsin (6 ng/µl).

Mass spectrometric analysis. Mass spectrometric analysis was performed by a hybrid Orbitrap LC-MS/MS instrument (Thermo Fisher).

Database searching. MS/MS spectra were searched using Mascot against the SwissProt database. Peptide tolerance was 20 ppm and fragment ion tolerance was 0.60 Da. Carbamidomethylation at cysteines was set as a fixed modification and oxidation of methionines was set as a variable modification.

Parsing using Scaffold. Mascot output files were further curated using Scaffold 3.5.1 analysis, resulting in a 0.2% protein false discovery rate (FDR) and a 5.3% peptide FDR. Further, identification of statistically significantly expressed proteins and heat maps were calculated using the R Statistical software package. Amino acid sequences corresponding to tryptic peptide masses identified in candidate proteins were subjected to the SCAFFOLD analysis software (for confidential protein identification) to rule out alternative protein identifications.

Pathway Analysis. Pathway Analysis was performed using Ingenuity Pathway Analysis application (Ingenuity Systems, CA).

ChIP-seq

TIC results were compared to CD133(-) control cells, for detection of genes with increased binding of Nanog. In parallel, isotype control antibody was used as a control. Briefly, cells were rinsed twice with PBS and treated with 1% formaldehyde for 20 min at room temperature to form DNA-protein crosslinks and sonicated to generate 200-500 bp chromatin fragments in size and incubated with anti-NANOG antibodies at 4 °C overnight. Protein A/G agarose beads were added to immune complexes at 4 °C. Immunoprecipitates were washed three times in wash buffer. ChIP DNA was purified by phenol-chloroform extraction and ethanol precipitation. NANOG ChIP for CD133- control cells and TICs was carried out as described in an instruction manual of Chromatin Immunoprecipitation Assay Kit (Cat#17-295: Millipore Inc., Temecula, CA). The DNA segments obtained by this method were sequenced and further subjected to bioinformatics analysis.

Bone marrow transplantation

Bone marrow transplantation (BMT) was performed as previously described (Dapito et al., 2012; Seki et al., 2007) with modification from traditional protocols as previsouly described (Kisseleva et al., 2006; Tsung et al., 2005). Briefly, after Kupffer cells were depleted (Van Rooijen and Sanders, 1994), mice were lethally irradiated with 750 cGy followed by tail vein intravenous injection of 10 million bone marrow cells collected from the femurs/tibias of donor mice since donor-derived bone marrow cells reconstitutes only 30% of Kupffer cells six months after BMT (Kennedy and Abkowitz, 1997). After 12 weeks BMT, efficiency of successful BMT was confirmed by harvesting splenocytes and determining LPS responsiveness using IL-6 mRNA induction by quantitative real-time PCR, as a readout. Diethynitrosamine (DEN) or vehicle (PBS) were intraperitoneally injected to mice 3 months after BMT.

Isolation of human TICs

We isolated CD133+/CD49f+ TICs from HCC tissues obtained from alcoholic patients with or without HCV infection, as previously described (Chen et al., 2013; Gripon et al., 2002). Fresh liver cancer tissues were collected from the USC transplant surgery unit in collaboration with Dr. Linda Sher. Following harvest, liver cancer specimens were immediately digested with collagenase and DNase to obtain cell suspensions, which were washed and adjusted to a concentration of 2×10^7 cells/ml. These cells were incubated with antibodies against CD133, CD49f, and CD45 (Becton Dickinson) and sorted by FACS to isolate CD133+CD49f+CD45- vs. CD133-CD49f+CD45- populations as previously described (Parent et al., 2004).

Bioinformatics analysis of mouse ChIP-seq data

Approximately, 20 million reads were aligned with the mm9 reference genome using Bowtie 2 (version 0.12.7) to generate around 18 million aligned reads with mapping quality ≥20, allowing only two mismatches per alignment (Li and Durbin, 2009). Only uniquely mapped reads were retained and redundant reads were filtered out. Further, each read was extended in the sequencing orientation to a total of 200 bases to infer the coverage at each genomic position. The genome was divided into non-overlapping windows 200 bp, and aligned reads were considered to be within a window of the midpoint of its estimated fragment. Mid-points in each window were counted, and empirical distributions of windows counts were created as described previously (Kim et al., 2013). The genomic bins, which contained statistically significant ChIP-Seq enrichment, were identified by comparison to a Poisson background model, assuming that background reads are spread randomly throughout the genome. In addition, fold-enrichment was calculated in CD133 + cells over CD133 – cells. The mapping output

files were also converted to browser-extensible data (BED) files. For visualization, wiggle tracks and TDF file were generated by computing mean read density over 25 bp bins of mouse genome with aligned and filtered reads from ChIP-seq data. Wiggle tracks were visualized in the IGV (Integrated Genomic Viewer)(Kim et al., 2013) as well as Seqmonk (Seqmonk v0.26.9). To assign ChIP-seq enriched regions to genes, a complete set of Refseq genes was downloaded from the UCSC genome dataset and, genes with enriched regions within 5 kb of their TSSs were called bound.

Gene ontology analysis

Genes which are differentially associated with NANOG in TICs or control cells were functionally analyzed in the context of gene ontology and molecular networks by using the Ingenuity pathway software (IPA; http://www.ingenuity.com). Differentially enriched genes were categorized into various functional groups (threshold P <0.05) and mapped to genetic networks and gene enrichments in specific pathways were calculated.

For Gene Ontology (GO) analysis, we used the known NANOG motif obtained from TRANSFAC to scan our NANOG ChIP-seq data set. In order to gain insight into the functions of genes, gene ontology (GO) analysis was performed. We compiled a list of GO terms that showed statistically significant over-representation for different classes of functions, such as proto-oncogenes, tumor suppression, transcription factors, cell cycle and translational regulation, house-keeping genes, developmentally regulated genes, immunity and anti-microbial defense genes. Quantitative data were analyzed using Partek and Ingenuity software.

Mitochondria labeling and measurement of ROS levels

To evaluate the status of mitochondria in TICs, the MitoTracker® Mitochondrion-selective probes for total mitochondrial mass (MitoTracker® Deep Red FM Invitrogen: M22426) and for oxidized state mitochondria (MitoSOX™ Red mitochondrial superoxide indicator) were added to the media, respectively, and cells subjected to FACS analyses. ROS labeling was performed as per the instructions for CellROX® Oxidative stress reagent Probes (CellROX® green reagent, Invitrogen C10444). In brief, the cells were incubated with staining solution (100 nM) in culture media at 37^{o}C for 30 minutes. After staining was complete, cells were washed with PBS and analyzed by fluorescent microscopy or flow cytometry.

Fluorescence microscopy

Cells were fixed in 3.7% formaldehyde for 10 min, blocked in 0.2% BSA for 5 min, and incubated with NANOG antibody (1:100; Abcam) and pAMPK antibody (1:100, Cell Signaling) in 0.1% Triton-X100 and 1 × PBS, pH 7.4 overnight at 4°C, followed by staining with FITC-conjugated rabbit anti-IgG Ab (1:500; Jackson ImmunoResearch) for 1 h. A LSM 5 Pa laser scanning microscope (Zeiss) was used to visualize mitochondrial morphology.

ATP production measurements

Relative ATP/cell assays were performed in 96-well plates. After cells were treated with inhibitors for 4 hr, culture media was removed. Cell Titer-Glo (100 µl: Promega) and CyQUANT(Invitrogen) were immediately added to each well. Luminescence and fluorescence readings were consecutively measured after room-temperature incubation for 10 min.

Determination of *cis*-elements for TLR4-induced *Nanog* promoter activation

To characterize the region required for TLR4-induced *Nanog* transcriptional induction, truncated promoter-luciferase constructs were used to test the functional role of predicted and known *cis*-elements, including E2F1 and NF-κB in its enhancer, and others on the promoter. Six constructs, carrying either a –5421/+50, -4828/+50, -2342/+50, –900/+50, –332/+50 or –153/+50 Nanog genomic fragment were generated or obtained from Dr. Paul Robson at the Genome Institute of Singapore and Dr. Takashi Tada in Kyoto University (Kuroda et al., 2005). To generate pGL3(–5421/+50) construct, -5421/-4828 PCR fragments was ligated into -4828/+50 construct. Each reporter was co-transfected with *Renilla* luciferase plasmid (SV40-Renilla) to normalize reporter activity to transfection efficiency of TLR4-transduced Huh7 cells. Two days after transfection, the cells were stimulated with LPS for 24 hr, and the cell lysate was analyzed by a dual luciferase assay.

NANOG enhancer and promoter assay following site-directed mutagenesis

To test the role of specific sequence elements within these regions, six mutant-luciferase plasmids were constructed by *in vitro* mutagenesis using QuikChange™ Site-Directed Mutagenesis Kit (Stratagene). For example, to examine the function of *E2F, NF-κB, p53, and IRF-3* elements on LPS-induced Nanog transcriptional activity, 3-bp mutations were generated within the corresponding core conserved regions by base substitution. To ascertain whether this region serves as a TLR4-responsive enhancer through the E2F1 and NF-κB interaction, we used reporter constructs with a 404-bp enhancer fragment inserted upstream or downstream of a *luciferase* reporter driven by an *Oct4* minimal promoter. These constructs were obtained from Dr. Ng Huck Hui of the Genome Institute of Singapore (Wu et al., 2006). *NF-κB and/or E2F* binding sites were mutated by introducing 3 bp substitutions (*Nanog Enh NF-κB and/or E2F mut* –Luc) and tested for enhancer activity in TLR4-Huh7 cells in the presence or absence of LPS stimulation. As a positive control, *Nanog* enhancer reporter or other control vector was co-transfected with E2F and c-MYC expression plasmid into Huh7 cells. The parental vector construct without the enhancer insert was used as a negative control. All luciferase activities were measured relative to the *Renilla luciferase*. Basal luciferase promoter activity was set arbitrarily to 100% for all comparisons.

***Cox6a2* and *Acadvl* promoter luciferase assay**

The promoter regions of *Cox6a2* and *Acadvl* were inserted into a pGL3 *Firefly* luciferase reporter vector as different truncation forms. *Cox6a2* promoter constructs with luciferase reporter were gifts of Dr. Moreadith (Wan and Moreadith, 1995). The luciferase assay was performed as per vendor instructions (Promega). Briefly, 1 μg of pGL3 luciferase plasmid was transfected with Fugene. A 100 ng of *Renilla* plasmid was co-transfected as an internal control. Cells were harvested 24 hr after transfection, and cell-free lysates were assayed for luciferase activity of cell lysate was measured with the dual-luciferase reporter assay kit (Promega) using a luminometer.

Lentiviral expression system

The cDNA for ACADVL was subcloned into the lentiviral vector and dsRed expression cassette. Two TLR4 or scrambled shRNAs in the lentiviral vector of pLKO were purchased from Sigma-Aldrich. The lentivirus overexpression vectors were purchased from Applied Biological Materials, and lentivirus shRNA vectors were purchased form Sigma-Aldrich. Lentivirus was made by transfecting 2×10^6 HEK293T cells with 10 μg of lentiviral vector, 6.5 μg pCMV-ΔR8.2 (packaging vector), and 3.5 μg pCMV-VSV-G (envelope vector) using Fugene (Roche). Forty eight hours later, medium was collected,

filtered, and concentrated using the Lenti-X concentrator (Clontech). Concentrated virus was added to TICs, followed by mixing for 2 hr at 37°C in the presence of 8 μg/μl polybrene in DMEM/F12 medium.

Reverse transcription and real-time PCR (qPCR)

Total RNA was extracted from the cells by RNeasy Mini kit (Qiagen). 1 μg of RNA was treated with DNase I (Invitrogen) and used for reverse-transcription (Omniscript RT kit, Qiagen). Quantitative real-time PCR was performed with Taqman Fast Advanced master mix (Invitrogen) using ABI 7900 system (Applied BioSystems). Taqman primers and probes for Actin (assay ID: Mm00607939_s1), Nanog (assay ID: Mm02384862_g1), Stat3 (assay ID: Mm01219775_m1), Esrrb (assay ID: Mm00442411_m1), Esr2 (assay ID: Mm00599821_m1), Pcx (assay ID: Mm00500992_m1), Atp6v1g2 (assay ID: Mm01159330_g1), Atp5d (assay ID: Mm00502864_m1), Atp5h (assay ID: Mm02392026_g1), Atp8b2 (assay ID: Mm01220121_m1), Acaa2 (assay ID: Mm00624282_m1), Cox15 (assay ID: Mm00523096_m1), Cox6a2 (assay ID: Mm00438295_g1), Ndufs2 (assay ID: Mm00467603_g1), Ndufv2 (assay ID: Mm01239727_m1), Uqcrfs1 (assay ID: Mm00481849_m1), Idh1 (assay ID: Mm00516030_m1), Idh2 (assay ID: Mm006124290_m1), Tet1 (assay ID: Mm01169087_m1), Tet2 (assay ID: Mm00524395_m1) and Tet3 (assay ID: Mm00805756_m1) were obtained from Applied Biosystems.

Immunoblotting

Cells were lysed in lysis buffer (50 mM Tris–HCl, pH 7.4, 150 mM NaCl, 1 mM EDTA, and 1% Triton-X100) containing 1 × protease inhibitor cocktail (Sigma). Protein (50 μg/sample) was resolved by 8–15% SDS–PAGE, transferred to nitrocellulose membranes, and incubated for 1 hr with 5% milk/TBS-T and overnight with primary Abs in 5% BSA. Abs used were: TLR4 (Santa Cruz), NANOG (Abcam), TAK1 (Cell Signaling), TBK1 (Cell signaling), AMPKs (Cell signaling), E2F1 (Cell signaling), pE2F1(Ser337) (Santa Cruz), pE2F1(Ser332) (Thermo Scientific), ACADVL (Santa Cruz). ECL Plus (GE Healthcare) was used for chemo-luminescent detection.

XF24 extracellular flux analyzer for measurement of cellular OCR and ECAR

To measure cellular bioenergetics using extracellular flux, a Seahorse XF96 Extracellular Flux Analyzer was used as following the published protocol (Ahfeldt et al., 2012; Ferrick et al., 2008) Functional assays of FAO and glycolysis in live cells showed that scrambled shRNA-transduced TICs had less glycolytic energetics (an embryonic pattern) (Onay-Besikci, 2006) as the baseline while Nanog-silenced TICs has similar glycolysis-dependency, but significant activation of FAO. Cells were plated in gelatin-coated XF 24-well cell culture microplates at 2–7.5 × 10^4 cells/well (Seahorse Bioscience) and incubated in pre-warmed unbuffered DMEM medium (DMEM containing 2 mM GlutaMAX, 1 mM sodium pyruvate, 1.85 g l^{-1} NaCl and 25 mM glucose) for 1 h. The oxygen consumption was measured by the XF24 extracellular flux analyzer (Seahorse Biosciences) in unbuffered DMEM assay medium supplemented with 1 mM pyruvate and 25 mM glucose after 45 to 60 min equilibration.

The characteristic function of mature hepatocytes is metabolism/thermogenesis, driven by the catabolic breakdown of lipids. To distinguish these tumor cells at a functional level, we analyzed the oxygen consumption rate (OCR) and extracellular acidification rate (ECAR) as previously described (Ahfeldt et al.). We observed that the basal OCR and ECAR rates were highest in the Nanog-silenced TICs. We added compounds that modulate mitochondrial function sequentially and measured the effect on OCR and ECAR after the addition of each compound. We first administered

oligomycin to determine ATP turnover and the degree of proton leakage. At the baseline, the Nanog-silenced TICs showed slightly elevated levels of proton leakage when compared to unprogrammed cells. After the addition of the electron transport chain decoupler (FCCP), we measured the maximal respiratory capacity. Nanog-silenced TICs showed significantly higher levels of OCR and ECAR when compared to the unprogrammed cells, whereas TICs did not. Finally, we administered antimycin to inhibit the flux of electrons through complex III and prevent oxygen consumption by the cytochrome c oxidase in the mitochondria as previously described (Ahfeldt et al.). For determination of individual ETC complex activities, mitochondrial biogenesis was profiled by adding perturbation drugs: 2 μM oligomycin, 0.5 μM FCCP and 5 μM antimycin A/rotenon, in succession. OCR for complexes II–IV was measured by first inhibiting complex I with rotenone; OCR for complexes III–IV was measured by first inhibiting complex II with FCCP; and OCR for complex IV was measured by first inhibiting complex III with antimycin. The Etomoxir (ETO, 100 μM)-sensitive component of oxygen consumption rate (OCR) represents FAO. Absolute values of OCR were expressed as pmol min^{-1} per 10^6 cells and mpH min^{-1} per 10^6 cells. OCR and ECAR were determined by plotting the oxygen tension and acidification of the medium in the chamber as a function of time and normalized to protein concentration (picomoles per minute per milligram), respectively (Ahfeldt et al.). OCR and ECAR were normalized by cell numbers in all experiments.

The ECAR was measured over time at 10 min intervals. The first three measurements were conducted to establish a baseline rate, followed by two measurements after the addition of oligomycin, an ATPase inhibitor (I). By uncoupling the proton gradient with FCCP, the maximum OCR rates were determined over the next two time intervals (II). By addition of glycolysis inhibitor (2-DG) or CPT1 inhibitor (ETO), the OCR rates were determined over the next two time intervals (III). Finally, at two time points, measurements were conducted after inhibition of the mitochondrial respiratory chain with antimycin/rotenon (IV).

Stable-isotope carbon labeling is traced for glutaminolysis analysis

To test the glutamine utilization, we incubated TICs in 1 mM of [U-$^{13}C_5$, 2,5-$^{15}N_2$]-glutamine (Cambridge Isotope Laboratory, Cat # CNLM-1275-H-PK) for 4 hr. When [U-$^{13}C_5$, 2,5-$^{15}N_2$]-glutamine is taken up by cells, it loses the ^{15}N on the 5th carbon and is converted to [U-$^{13}C_5$, 2-^{15}N]-glutamate, which loses the ^{15}N on the 2nd carbon and becomes [U-$^{13}C_5$]-glutamate after rapid equilibration with TCA cycle intermediate α-ketoglutarate. When glutamine and glutamate were analyzed by gas chromatography mass spectrometry (GC-MS) using electronic impact ionization (EI), their TFA derivatives give rise to a C2-C4 (m/z 152) and C2-C5 (m/z 198) fragments (Lee et al., 1996). Thus, the [U-$^{13}C_5$, 2-^{15}N]-glutamate has a C2-C4 fragment of m/z 156 (M4; contains 3x^{13}C and a ^{15}N) and a C2-C5 fragment of m/z 204 (M5; contains 4x^{13}C and a ^{15}N), which represent the relative abundance of glutamine taken up by the TICs. On the other hand, [U-$^{13}C_5$]-glutamate has a C2-C4 fragment of m/z 155 (M3; contains 3x^{13}C) and a C2-C5 fragment of m/z 204 (M4; contains 4x^{13}C). When the [U-$^{13}C_5$]-glutamate enters TCA cycle metabolism, it will gradually lose the ^{13}C carbon after each cycle and generate M2, M1, and M0 C2-C4 fragment and M3, M2, M1, and M0 C2-C5 fragment, which represent the TCA cycle activity (Lee et al., 1996). Vigatroin was added in cell culture media and incubated for 20 hr then 1mM [U-$^{13}C_5$, 2-^{15}N]-glutamate was added. The sh-TLR4 or sh-Nanog silencing reduces glutamine uptake by the TICs as evident by decreased percentage of M3 and M4 glutamate (C2-C4) and M4 and M5 (C2-C5) fragments.

***In vivo* rescue experiments of OXPHOS gene and inhibition of FAO by implantation of TICs into immunocompromised mice**

The effect of restoration of an OXPHOS gene and/or inhibition of FAO for effect on tumorigenicity of TICs in a xenograft model was examined. Cryopreserved human TICs obtained from liver tumors were tested for tumorigenicity in NOG mice. Prior to implantation, these cells were expanded through several passages and infected with the lentiviral vector expressing *Cox6a2* cDNA and *dsRed* (as a fluorescence tracing marker for *in vivo* imaging) (MOI 10). Ten days post-lentivirus infection, TICs (1×10^4) were subcutaneously injected into 6-8-week-old NOG. Tumor growth was monitored and palpable tumors were measured by caliper every 4 days for 44 days.

Statistical Considerations

Log-rank tests and Cox regression was used to determine if differences between groups were significant ($\alpha = 0.05$). The growth of liver tumors was monitored by caliper. The normal chow fed mice served as the control to confirm that the alcohol Western diet had the intended effect. Data are presented as mean±S.D. A two-tailed t-test was used for most comparisons, with $p<0.05$ considered statistically significant. For the parameters measured in the experiment above, two-tailed non-paired Student's *t*-test was used for comparison between two groups, and *p* values less than 0.05 were considered significant. ANOVA and Fisher's test was used for comparison of more than two groups.

Supplemental References

Ahfeldt, T., Schinzel, R.T., Lee, Y.K., Hendrickson, D., Kaplan, A., Lum, D.H., Camahort, R., Xia, F., Shay, J., Rhee, E.P.*, et al.* Programming human pluripotent stem cells into white and brown adipocytes. Nat Cell Biol *14*, 209-219.

Ahfeldt, T., Schinzel, R.T., Lee, Y.K., Hendrickson, D., Kaplan, A., Lum, D.H., Camahort, R., Xia, F., Shay, J., Rhee, E.P.*, et al.* (2012). Programming human pluripotent stem cells into white and brown adipocytes. Nat Cell Biol *14*, 209-219.

Aoyama, T., Souri, M., Ueno, I., Kamijo, T., Yamaguchi, S., Rhead, W.J., Tanaka, K., and Hashimoto, T. (1995). Cloning of human very-long-chain acyl-coenzyme A dehydrogenase and molecular characterization of its deficiency in two patients. Am J Hum Genet *57*, 273-283.

Bauer, A.K., Dixon, D., DeGraff, L.M., Cho, H.Y., Walker, C.R., Malkinson, A.M., and Kleeberger, S.R. (2005). Toll-like receptor 4 in butylated hydroxytoluene-induced mouse pulmonary inflammation and tumorigenesis. J Natl Cancer Inst *97*, 1778-1781.

Campanero, M.R., Armstrong, M., and Flemington, E. (1999). Distinct cellular factors regulate the c-myb promoter through its E2F element. Mol Cell Biol *19*, 8442-8450.

Caro, P., Kishan, A.U., Norberg, E., Stanley, I.A., Chapuy, B., Ficarro, S.B., Polak, K., Tondera, D., Gounarides, J., Yin, H.*, et al.* (2012). Metabolic signatures uncover distinct targets in molecular subsets of diffuse large B cell lymphoma. Cancer Cell *22*, 547-560.

Chen, C.L., Tsukamoto, H., Liu, J.C., Kashiwabara, C., Feldman, D., Sher, L., Dooley, S., French, S.W., Mishra, L., Petrovic, L.*, et al.* (2013). Reciprocal regulation by TLR4 and TGF-beta in tumor-initiating stem-like cells. The Journal of clinical investigation *123*, 2832-2849.

Dapito, D.H., Mencin, A., Gwak, G.Y., Pradere, J.P., Jang, M.K., Mederacke, I., Caviglia, J.M., Khiabanian, H., Adeyemi, A., Bataller, R.*, et al.* (2012). Promotion of hepatocellular carcinoma by the intestinal microbiota and TLR4. Cancer Cell *21*, 504-516.

DeBerardinis, R.J., Mancuso, A., Daikhin, E., Nissim, I., Yudkoff, M., Wehrli, S., and Thompson, C.B. (2007). Beyond aerobic glycolysis: transformed cells can engage in glutamine metabolism that exceeds the requirement for protein and nucleotide synthesis.

Proceedings of the National Academy of Sciences of the United States of America *104*, 19345-19350.
Diehl, A.M., and Hoek, J.B. (1999). Mitochondrial uncoupling: role of uncoupling protein anion carriers and relationship to thermogenesis and weight control "the benefits of losing control". J Bioenerg Biomembr *31*, 493-506.
Fagan, R., Flint, K.J., and Jones, N. (1994). Phosphorylation of E2F-1 modulates its interaction with the retinoblastoma gene product and the adenoviral E4 19 kDa protein. Cell *78*, 799-811.
Fan, W., Morinaga, H., Kim, J.J., Bae, E., Spann, N.J., Heinz, S., Glass, C.K., and Olefsky, J.M. (2010). FoxO1 regulates Tlr4 inflammatory pathway signalling in macrophages. EMBO J *29*, 4223-4236.
Ferrick, D.A., Neilson, A., and Beeson, C. (2008). Advances in measuring cellular bioenergetics using extracellular flux. Drug Discov Today *13*, 268-274.
Fukata, M., Chen, A., Vamadevan, A.S., Cohen, J., Breglio, K., Krishnareddy, S., Hsu, D., Xu, R., Harpaz, N., Dannenberg, A.J*., et al.* (2007). Toll-like receptor-4 promotes the development of colitis-associated colorectal tumors. Gastroenterology *133*, 1869-1881.
Gan, B., Hu, J., Jiang, S., Liu, Y., Sahin, E., Zhuang, L., Fletcher-Sananikone, E., Colla, S., Wang, Y.A., Chin, L*., et al.* (2010). Lkb1 regulates quiescence and metabolic homeostasis of haematopoietic stem cells. Nature *468*, 701-704.
Giordano, A., Calvani, M., Petillo, O., Grippo, P., Tuccillo, F., Melone, M.A., Bonelli, P., Calarco, A., and Peluso, G. (2005). tBid induces alterations of mitochondrial fatty acid oxidation flux by malonyl-CoA-independent inhibition of carnitine palmitoyltransferase-1. Cell Death Differ *12*, 603-613.
Gripon, P., Rumin, S., Urban, S., Le Seyec, J., Glaise, D., Cannie, I., Guyomard, C., Lucas, J., Trepo, C., and Guguen-Guillouzo, C. (2002). Infection of a human hepatoma cell line by hepatitis B virus. Proceedings of the National Academy of Sciences of the United States of America *99*, 15655-15660.
Gurumurthy, S., Xie, S.Z., Alagesan, B., Kim, J., Yusuf, R.Z., Saez, B., Tzatsos, A., Ozsolak, F., Milos, P., Ferrari, F*., et al.* (2010). The Lkb1 metabolic sensor maintains haematopoietic stem cell survival. Nature *468*, 659-663.
Haluzik, M., Gavrilova, O., and LeRoith, D. (2004). Peroxisome proliferator-activated receptor-alpha deficiency does not alter insulin sensitivity in mice maintained on regular or high-fat diet: hyperinsulinemic-euglycemic clamp studies. Endocrinology *145*, 1662-1667.
Harbour, J.W., and Dean, D.C. (2000). The Rb/E2F pathway: expanding roles and emerging paradigms. Genes & development *14*, 2393-2409.
Huynh, H., Ngo, V.C., Koong, H.N., Poon, D., Choo, S.P., Thng, C.H., Chow, P., Ong, H.S., Chung, A., and Soo, K.C. (2009). Sorafenib and rapamycin induce growth suppression in mouse models of hepatocellular carcinoma. J Cell Mol Med *13*, 2673-2683.
Ito, K., Carracedo, A., Weiss, D., Arai, F., Ala, U., Avigan, D.E., Schafer, Z.T., Evans, R.M., Suda, T., Lee, C.H*., et al.* (2012). A PML-PPAR-delta pathway for fatty acid oxidation regulates hematopoietic stem cell maintenance. Nat Med *18*, 1350-1358.
Ito, K., Hirao, A., Arai, F., Matsuoka, S., Takubo, K., Hamaguchi, I., Nomiyama, K., Hosokawa, K., Sakurada, K., Nakagata, N*., et al.* (2004). Regulation of oxidative stress by ATM is required for self-renewal of haematopoietic stem cells. Nature *431*, 997-1002.
Ito, K., Hirao, A., Arai, F., Takubo, K., Matsuoka, S., Miyamoto, K., Ohmura, M., Naka, K., Hosokawa, K., Ikeda, Y*., et al.* (2006). Reactive oxygen species act through p38 MAPK to limit the lifespan of hematopoietic stem cells. Nat Med *12*, 446-451.
Jiang, J., Chan, Y.S., Loh, Y.H., Cai, J., Tong, G.Q., Lim, C.A., Robson, P., Zhong, S., and Ng, H.H. (2008). A core Klf circuitry regulates self-renewal of embryonic stem cells. Nat Cell Biol *10*, 353-360.
Johnson, D.G., and Schneider-Broussard, R. (1998). Role of E2F in cell cycle control and cancer. Front Biosci *3*, d447-448.

Kennedy, D.W., and Abkowitz, J.L. (1997). Kinetics of central nervous system microglial and macrophage engraftment: analysis using a transgenic bone marrow transplantation model. Blood *90*, 986-993.
Kersten, S., Seydoux, J., Peters, J.M., Gonzalez, F.J., Desvergne, B., and Wahli, W. (1999). Peroxisome proliferator-activated receptor alpha mediates the adaptive response to fasting. The Journal of clinical investigation *103*, 1489-1498.
Khacho, M., Tarabay, M., Patten, D., Khacho, P., MacLaurin, J.G., Guadagno, J., Bergeron, R., Cregan, S.P., Harper, M.E., Park, D.S.*, et al.* (2014). Acidosis overrides oxygen deprivation to maintain mitochondrial function and cell survival. Nat Commun *5*, 3550.
Kim, K., Punj, V., Choi, J., Heo, K., Kim, J.M., Laird, P.W., and An, W. (2013). Gene dysregulation by histone variant H2A.Z in bladder cancer. Epigenetics Chromatin *6*, 34.
Kisseleva, T., Uchinami, H., Feirt, N., Quintana-Bustamante, O., Segovia, J.C., Schwabe, R.F., and Brenner, D.A. (2006). Bone marrow-derived fibrocytes participate in pathogenesis of liver fibrosis. J Hepatol *45*, 429-438.
Klingenberg, M., and Huang, S.G. (1999). Structure and function of the uncoupling protein from brown adipose tissue. Biochim Biophys Acta *1415*, 271-296.
Krauss, S., Zhang, C.Y., and Lowell, B.B. (2005). The mitochondrial uncoupling-protein homologues. Nat Rev Mol Cell Biol *6*, 248-261.
Kuroda, T., Tada, M., Kubota, H., Kimura, H., Hatano, S.Y., Suemori, H., Nakatsuji, N., and Tada, T. (2005). Octamer and Sox elements are required for transcriptional cis regulation of Nanog gene expression. Mol Cell Biol *25*, 2475-2485.
Kurtz, D.M., Rinaldo, P., Rhead, W.J., Tian, L., Millington, D.S., Vockley, J., Hamm, D.A., Brix, A.E., Lindsey, J.R., Pinkert, C.A.*, et al.* (1998). Targeted disruption of mouse long-chain acyl-CoA dehydrogenase gene reveals crucial roles for fatty acid oxidation. Proceedings of the National Academy of Sciences of the United States of America *95*, 15592-15597.
Lamonte, G., Tang, X., Chen, J.L., Wu, J., Ding, C.K., Keenan, M.M., Sangokoya, C., Kung, H.N., Ilkayeva, O., Boros, L.G.*, et al.* (2013). Acidosis induces reprogramming of cellular metabolism to mitigate oxidative stress. Cancer Metab *1*, 23.
Lee, W.N. (1996). Stable isotopes and mass isotopomer study of fatty acid and cholesterol synthesis. A review of the MIDA approach. Adv Exp Med Biol *399*, 95-114.
Lee, W.N., Edmond, J., Bassilian, S., and Morrow, J.W. (1996). Mass isotopomer study of glutamine oxidation and synthesis in primary culture of astrocytes. Dev Neurosci *18*, 469-477.
Li, H., and Durbin, R. (2009). Fast and accurate short read alignment with Burrows-Wheeler transform. Bioinformatics *25*, 1754-1760.
Liang, J., Wan, M., Zhang, Y., Gu, P., Xin, H., Jung, S.Y., Qin, J., Wong, J., Cooney, A.J., Liu, D.*, et al.* (2008). Nanog and Oct4 associate with unique transcriptional repression complexes in embryonic stem cells. Nat Cell Biol *10*, 731-739.
Lim, C.A., Yao, F., Wong, J.J., George, J., Xu, H., Chiu, K.P., Sung, W.K., Lipovich, L., Vega, V.B., Chen, J.*, et al.* (2007). Genome-wide mapping of RELA(p65) binding identifies E2F1 as a transcriptional activator recruited by NF-kappaB upon TLR4 activation. Mol Cell *27*, 622-635.
Lin, T., Chao, C., Saito, S., Mazur, S.J., Murphy, M.E., Appella, E., and Xu, Y. (2005). p53 induces differentiation of mouse embryonic stem cells by suppressing Nanog expression. Nat Cell Biol *7*, 165-171.
Lundberg, A.S., and Weinberg, R.A. (1998). Functional inactivation of the retinoblastoma protein requires sequential modification by at least two distinct cyclin-cdk complexes. Mol Cell Biol *18*, 753-761.
Machida, K., Tsukamoto, H., Liu, J.C., Han, Y.P., Govindarajan, S., Lai, M.M., Akira, S., and Ou, J.H. (2010). c-Jun mediates hepatitis C virus hepatocarcinogenesis through signal transducer and activator of transcription 3 and nitric oxide-dependent impairment of oxidative DNA repair. Hepatology *52*, 480-492.

Machida, K., Tsukamoto, H., Mkrtchyan, H., Duan, L., Dynnyk, A., Liu, H.M., Asahina, K., Govindarajan, S., Ray, R., Ou, J.H., *et al.* (2009). Toll-like receptor 4 mediates synergism between alcohol and HCV in hepatic oncogenesis involving stem cell marker Nanog. Proceedings of the National Academy of Sciences of the United States of America *106*, 1548-1553.
Mathurin, P., Deng, Q.G., Keshavarzian, A., Choudhary, S., Holmes, E.W., and Tsukamoto, H. (2000). Exacerbation of alcoholic liver injury by enteral endotoxin in rats. Hepatology *32*, 1008-1017.
Mittal, D., Saccheri, F., Venereau, E., Pusterla, T., Bianchi, M.E., and Rescigno, M. (2010). TLR4-mediated skin carcinogenesis is dependent on immune and radioresistant cells. Embo J *29*, 2242-2252.
Nakada, D., Saunders, T.L., and Morrison, S.J. (2010). Lkb1 regulates cell cycle and energy metabolism in haematopoietic stem cells. Nature *468*, 653-658.
Onay-Besikci, A. (2006). Regulation of cardiac energy metabolism in newborn. Mol Cell Biochem *287*, 1-11.
Parent, R., Marion, M.J., Furio, L., Trepo, C., and Petit, M.A. (2004). Origin and characterization of a human bipotent liver progenitor cell line. Gastroenterology *126*, 1147-1156.
Paumen, M.B., Ishida, Y., Han, H., Muramatsu, M., Eguchi, Y., Tsujimoto, Y., and Honjo, T. (1997). Direct interaction of the mitochondrial membrane protein carnitine palmitoyltransferase I with Bcl-2. Biochem Biophys Res Commun *231*, 523-525.
Pestereva, E., Kanakasabai, S., and Bright, J.J. (2012). PPARgamma agonists regulate the expression of stemness and differentiation genes in brain tumour stem cells. British journal of cancer *106*, 1702-1712.
Quintens, R., Singh, S., Lemaire, K., De Bock, K., Granvik, M., Schraenen, A., Vroegrijk, I.O., Costa, V., Van Noten, P., Lambrechts, D., *et al.* (2013). Mice deficient in the respiratory chain gene Cox6a2 are protected against high-fat diet-induced obesity and insulin resistance. PLoS One *8*, e56719.
Rodda, D.J., Chew, J.L., Lim, L.H., Loh, Y.H., Wang, B., Ng, H.H., and Robson, P. (2005). Transcriptional regulation of nanog by OCT4 and SOX2. J Biol Chem *280*, 24731-24737.
Saberi, M., Woods, N.B., de Luca, C., Schenk, S., Lu, J.C., Bandyopadhyay, G., Verma, I.M., and Olefsky, J.M. (2009). Hematopoietic cell-specific deletion of toll-like receptor 4 ameliorates hepatic and adipose tissue insulin resistance in high-fat-fed mice. Cell Metab *10*, 419-429.
Samudio, I., Harmancey, R., Fiegl, M., Kantarjian, H., Konopleva, M., Korchin, B., Kaluarachchi, K., Bornmann, W., Duvvuri, S., Taegtmeyer, H., *et al.* (2010). Pharmacologic inhibition of fatty acid oxidation sensitizes human leukemia cells to apoptosis induction. The Journal of clinical investigation *120*, 142-156.
Sato, A., Okada, M., Shibuya, K., Watanabe, E., Seino, S., Narita, Y., Shibui, S., Kayama, T., and Kitanaka, C. (2014). Pivotal role for ROS activation of p38 MAPK in the control of differentiation and tumor-initiating capacity of glioma-initiating cells. Stem Cell Res *12*, 119-131.
Seki, E., De Minicis, S., Osterreicher, C.H., Kluwe, J., Osawa, Y., Brenner, D.A., and Schwabe, R.F. (2007). TLR4 enhances TGF-beta signaling and hepatic fibrosis. Nat Med *13*, 1324-1332.
Siddique, H.R., and Saleem, M. (2012). Role of BMI1, a stem cell factor, in cancer recurrence and chemoresistance: preclinical and clinical evidences. Stem Cells *30*, 372-378.
Spender, L.C., and Inman, G.J. (2009). TGF-beta induces growth arrest in Burkitt lymphoma cells via transcriptional repression of E2F-1. J Biol Chem *284*, 1435-1442.
Storm, M.P., Bone, H.K., Beck, C.G., Bourillot, P.Y., Schreiber, V., Damiano, T., Nelson, A., Savatier, P., and Welham, M.J. (2007). Regulation of Nanog expression by

phosphoinositide 3-kinase-dependent signaling in murine embryonic stem cells. J Biol Chem *282*, 6265-6273.
Suzuki, A., Raya, A., Kawakami, Y., Morita, M., Matsui, T., Nakashima, K., Gage, F.H., Rodriguez-Esteban, C., and Izpisua Belmonte, J.C. (2006). Nanog binds to Smad1 and blocks bone morphogenetic protein-induced differentiation of embryonic stem cells. Proceedings of the National Academy of Sciences of the United States of America *103*, 10294-10299.
Takubo, K., Nagamatsu, G., Kobayashi, C.I., Nakamura-Ishizu, A., Kobayashi, H., Ikeda, E., Goda, N., Rahimi, Y., Johnson, R.S., Soga, T.*, et al.* (2013). Regulation of glycolysis by Pdk functions as a metabolic checkpoint for cell cycle quiescence in hematopoietic stem cells. Cell Stem Cell *12*, 49-61.
Tikhanovich, I., Kuravi, S., Campbell, R.V., Kharbanda, K.K., Artigues, A., Villar, M.T., and Weinman, S.A. (2014). Regulation of FOXO3 by phosphorylation and methylation in hepatitis C virus infection and alcohol exposure. Hepatology *59*, 58-70.
Tsung, A., Hoffman, R.A., Izuishi, K., Critchlow, N.D., Nakao, A., Chan, M.H., Lotze, M.T., Geller, D.A., and Billiar, T.R. (2005). Hepatic ischemia/reperfusion injury involves functional TLR4 signaling in nonparenchymal cells. Journal of immunology *175*, 7661-7668.
Valent, P., Bonnet, D., De Maria, R., Lapidot, T., Copland, M., Melo, J.V., Chomienne, C., Ishikawa, F., Schuringa, J.J., Stassi, G.*, et al.* (2012). Cancer stem cell definitions and terminology: the devil is in the details. Nat Rev Cancer *12*, 767-775.
Van Heek, M., Compton, D.S., France, C.F., Tedesco, R.P., Fawzi, A.B., Graziano, M.P., Sybertz, E.J., Strader, C.D., and Davis, H.R., Jr. (1997). Diet-induced obese mice develop peripheral, but not central, resistance to leptin. The Journal of clinical investigation *99*, 385-390.
Van Rooijen, N., and Sanders, A. (1994). Liposome mediated depletion of macrophages: mechanism of action, preparation of liposomes and applications. Journal of immunological methods *174*, 83-93.
Vickers, A.E. (2009). Characterization of hepatic mitochondrial injury induced by fatty acid oxidation inhibitors. Toxicol Pathol *37*, 78-88.
Wan, B., and Moreadith, R.W. (1995). Structural characterization and regulatory element analysis of the heart isoform of cytochrome c oxidase VIa. J Biol Chem *270*, 26433-26440.
Wang, E., Bhattacharyya, S., Szabolcs, A., Rodriguez-Aguayo, C., Jennings, N.B., Lopez-Berestein, G., Mukherjee, P., Sood, A.K., and Bhattacharya, R. (2011). Enhancing chemotherapy response with Bmi-1 silencing in ovarian cancer. PLoS One *6*, e17918.
Weinberg, F., Hamanaka, R., Wheaton, W.W., Weinberg, S., Joseph, J., Lopez, M., Kalyanaraman, B., Mutlu, G.M., Budinger, G.R., and Chandel, N.S. (2010). Mitochondrial metabolism and ROS generation are essential for Kras-mediated tumorigenicity. Proceedings of the National Academy of Sciences of the United States of America *107*, 8788-8793.
Wu da, Y., and Yao, Z. (2005). Isolation and characterization of the murine Nanog gene promoter. Cell Res *15*, 317-324.
Wu, Q., Chen, X., Zhang, J., Loh, Y.H., Low, T.Y., Zhang, W., Zhang, W., Sze, S.K., Lim, B., and Ng, H.H. (2006). Sall4 interacts with Nanog and co-occupies Nanog genomic sites in embryonic stem cells. J Biol Chem *281*, 24090-24094.
Wu, Z., Puigserver, P., Andersson, U., Zhang, C., Adelmant, G., Mootha, V., Troy, A., Cinti, S., Lowell, B., Scarpulla, R.C.*, et al.* (1999). Mechanisms controlling mitochondrial biogenesis and respiration through the thermogenic coactivator PGC-1. Cell *98*, 115-124.
Zhang, D., Liu, Z.X., Choi, C.S., Tian, L., Kibbey, R., Dong, J., Cline, G.W., Wood, P.A., and Shulman, G.I. (2007). Mitochondrial dysfunction due to long-chain Acyl-CoA dehydrogenase deficiency causes hepatic steatosis and hepatic insulin resistance.

Proceedings of the National Academy of Sciences of the United States of America *104*, 17075-17080.
Zhang, J., Khvorostov, I., Hong, J.S., Oktay, Y., Vergnes, L., Nuebel, E., Wahjudi, P.N., Setoguchi, K., Wang, G., Do, A.*, et al.* (2011). UCP2 regulates energy metabolism and differentiation potential of human pluripotent stem cells. EMBO J *30*, 4860-4873.
Zhang, L.F., Ding, J.H., Yang, B.Z., He, G.C., and Roe, C. (2003). Characterization of the bidirectional promoter region between the human genes encoding VLCAD and PSD-95. Genomics *82*, 660-668.

Supplementary Table 1 (Related to Fig. 1). Differentially expressed 48 Signature proteins in three groups

SwissProt (name)	Accession no	Ensembl Gene	Ethano+Ns5a vs Thanol+WT		Ethanol+Core vs Ethanol+WT		WD+Core vs WD+WT	
			FC	Regulation	FC	Regulation	FC	Regulation
HMCS2	P54869	ENSMUSG00000027875	0.888888889	DOWN	0.857142857	DOWN	2.222222222	UP
HSP7C	P63017	ENSMUSG00000015656	0.833333333	DOWN	4.666666667	UP	0.6	DOWN
DAK	Q8VC30	ENSMUSG00000034371	0.666666667	DOWN	2.75	UP	0.533333333	DOWN
METK1	Q91X83	ENSMUSG00000037798	0.666666667	DOWN	10	UP	0.666666667	DOWN
HS90B	P11499	ENSMUSG00000023944	0.6	DOWN	2.666666667	UP	0.6	DOWN
AATM	P05202	ENSMUSG00000031672	0.833333333	DOWN	3	UP	1.4	UP
TPIS	P17751	ENSMUSG00000023456	0.777777778	DOWN	2.333333333	UP	1.333333333	UP
HPPD	P49429	ENSMUSG00000029445	0.75	DOWN	2	UP	2	UP
ALDH2	P47738	ENSMUSG00000029455	0.733333333	DOWN	2	UP	1.5625	UP
PRDX5	P99029	ENSMUSG00000024953	0.666666667	DOWN	3	UP	4	UP
ACTB	P60710	ENSMUSG00000029580	0.65	DOWN	2.6	UP	1.545454545	UP
MIF	P34884	ENSMUSG00000033307	0.571428571	DOWN	1.25	UP	1.25	UP
ETFB	Q9DCW4	ENSMUSG00000004610	0.5	DOWN	1.428571429	UP	1.5	UP
UBIQ	P62991	ENSMUSG00000008348	0.5	DOWN	3.5	UP	1.375	UP
F16P1	Q9QXD6	ENSMUSG00000069805	10	UP	0.75	DOWN	0.636363636	DOWN
FTHFD	Q8R0Y6	ENSMUSG00000030088	2.294117647	UP	0.666666667	DOWN	0.846153846	DOWN
BLVRB	Q923D2	ENSMUSG00000040466	1.25	UP	0.666666667	DOWN	0.714285714	DOWN
IREB1	P28271	ENSMUSG00000028405	4	UP	0.5	DOWN	2	UP
PROF1	P62962	ENSMUSG00000018293	4	UP	0.8	DOWN	1.25	UP
CAH3	P16015	ENSMUSG00000027559	1.863636364	UP	0.566666667	DOWN	1.4	UP
FTCD	Q91XD4	ENSMUSG00000001155	1.5	UP	0.5	DOWN	1.5	UP
HBB1	P02088	ENSMUSG00000052305	1.341176471	UP	0.698412698	DOWN	1.824561404	UP
CPSM	Q8C196	ENSMUSG00000025991	1.333333333	UP	0.954887218	DOWN	1.27388535	UP
GFRP	P99025	ENSMUSG00000046814	3	UP	1.5	UP	0.5	DOWN
ASSY	P16460	ENSMUSG00000076441	2.083333333	UP	1.125	UP	0.785714286	DOWN
ARLY	Q91YI0	ENSMUSG00000025533	2	UP	4.4	UP	0.75	DOWN
INMT	P40936	ENSMUSG00000003477	2	UP	2.5	UP	0.75	DOWN
PHS	P61458	ENSMUSG00000020098	2	UP	2	UP	0.75	DOWN
ENOA	P17182	ENSMUSG00000059040	1.75	UP	2	UP	0.818181818	DOWN
FABPL	P12710	ENSMUSG00000054422	1.666666667	UP	1.259259259	UP	0.888888889	DOWN
CBR1	P48758	ENSMUSG00000051483	1.5	UP	6	UP	0.666666667	DOWN
DHB5	P70694	ENSMUSG00000021210	8	UP	3	UP	2	UP
GPX1	P11352	ENSMUSG00000063856	5	UP	5	UP	2.333333333	UP
PARK7	Q99LX0	ENSMUSG00000028964	5	UP	1.333333333	UP	2	UP
PRDX6	O08709	ENSMUSG00000026701	4.5	UP	3.666666667	UP	1.25	UP
CATA	P24270	ENSMUSG00000027187	4	UP	3	UP	2	UP
THIM	Q8BWT1	ENSMUSG00000036880	3.5	UP	2.5	UP	1.222222222	UP
MAAI	Q9WVL0	ENSMUSG00000021033	3.2	UP	1.416666667	UP	1.8	UP
KHK	P97328	ENSMUSG00000029162	3	UP	2	UP	1.5	UP
ABHEB	Q8VCR7	ENSMUSG00000042073	2	UP	2.5	UP	1.666666667	UP
GLRX1	Q9QUH0	ENSMUSG00000021591	2	UP	2	UP	2	UP
K2C5	Q922U2	ENSMUSG00000061527	2	UP	1.5	UP	3	UP
PEBP1	P70296	ENSMUSG00000032959	2	UP	2	UP	1.333333333	UP
EF1A1	P10126	ENSMUSG00000037742	1.8	UP	1.25	UP	3	UP
ARGI1	Q61176	ENSMUSG00000019987	1.777777778	UP	3	UP	1.833333333	UP
GSTP1	P19157	ENSMUSG00000060803	1.357142857	UP	1.714285714	UP	1.333333333	UP
ACBP	P31786	ENSMUSG00000026385	1.333333333	UP	6	UP	1.333333333	UP
G3P	P16858	ENSMUSG00000057666	1.25	UP	2	UP	1.375	UP

Supplemental Table 2 (Related to Fig. 1 and 2) Average scores of liver histology in HCV *Core* and/or *NS5A* Tg mice fed with the ethanol or Western diet (WD) for 12 months.

	Diet	Fatty liver (0-4+)	Spotty necrosis (0-2+)	Inflammation (0-2+)
sh-*Nanog*	LFD+Dextrin	0.3	0	0.1
*Alb-Cre;*sh-*Nanog*	LFD+Dextrin	0.3	0	0.1
sh-*Nanog;NS5A* Tg	LFD+Dextrin	0.4	0.1	0.1
Alb-Cre;sh-*Nanog*;*NS5A* Tg	LFD+Dextrin	0.3	0	0.2
sh-*Nanog*	EtOH+WD	2.4	0.4	0.4
Alb-Cre;sh-*Nanog*	EtOH+WD	1.7	0.2	0.8
sh-*Nanog;NS5A* Tg	EtOH+WD	3.4	0.9	1.6
*Alb-Cre;*sh-*Nanog;NS5A* Tg	EtOH+WD	1.5	0.3	0.5
Non-Tg	Dextrin	0.3	0.1	0
Core Tg	Dextrin	0.4	0.1	0.2
Core/NS5A Tg	Dextrin	0.5	0.3	0.1
Tlr4-/-	Dextrin	0.2	0	0.4
Tlr4-/- Core Tg	Dextrin	0.5	0.1	0.1
Tlr4-/- Core/NS5A Tg	Dextrin	0.4	0.2	0.1
Non-Tg	LFD	0.2	0	0.1
Core Tg	LFD	0.4	0.1	0.2
Core/NS5A Tg	LFD	0.5	0.2	0.3
Tlr4-/- Tg	LFD	0.2	0	0.5
Tlr4-/- Core Tg	LFD	0.3	0.2	0.3
Tlr4 -/- Core/NS5A Tg	LFD	0.3	0.1	0.4
Non-Tg	Ethanol	1.0	0.1	0.2
Core Tg	Ethanol	1.3	0.2	0.9
Core/Ns5a Tg	Ethanol	1.9	0.4	1.1
Tlr4-/-	Ethanol	0.4	0.1	0.4
Tlr4-/- Core Tg	Ethanol	0.8	0.2	0.6
Tlr4-/- Core/NS5A Tg	Ethanol	1.1	0.2	0.8
Non-Tg	WD	2.2	0.5	0.7
Core Tg	WD	3.3	0.6	1.1
Core/NS5A Tg	WD	3.4	0.7	1.3
Tlr4-/- Tg	WD	1.0	0.1	0.6
Tlr4-/- Core Tg	WD	1.3	0.2	0.7
Tlr4 -/- Core/NS5A Tg	WD	1.6	0.3	0.8

Fatty liver, 2+:25%~50% heaptocytes with fat; 3+:50%~75% with fat; 4+: >75% with fat.
Submassive necrosis/inflammation, 1+: lesions encompassing less than 1/3 acinus; 2+: lesions larger than whole acini.
LFD: Low fat diet
HCFD: High-cholesterol high-fat diet